that DOX was efficiently encapsulated into liposomes and the loading efficacy was more than 98% reproducibly. Particle size and zeta-potential of the DOX-encapsulated liposomes were determined by dynamic light scattering spectrophotometer (Zetasizer Nano, Malvern Instruments Ltd., Worcestershire, UK), and were 103.3±8.0 nm and −3.85±0.36 mV, respectively.

2.7. Animals and preparation of tumor-bearing mice model

Male BALB/c mice (6–7 weeks) for the inoculation of C26/control and C26/DOX were purchased from Charles River Laboratories Inc. (Wilmington, MA) and maintained at 25 °C and 55% of humidity with free access to standard chow and water. To prepare tumor-bearing mice, 10^6 cells were subcutaneously inoculated into the back of mice. Our investigations were performed after approval by our local ethical committee at Okayama University and in accordance with Principles of Laboratory Animal Care (NIH publication #85-23).

2.8. in vivo anti-tumor activity

When the tumor volume reached about 100 mm^3 in volume, PEG liposomal DOX was intravenously administered through the tail vein with a dose of either 2 or 4 mg/kg as DOX ($n=5$). Saline solution was injected into control group ($n=5$). The tumor volume was measured every other day with a caliper in two dimensions, and tumor volume was calculated using the following equation (Eq. (3)) [7]:

$$\text{Volume}(mm^3) = \text{longer diameter} \times (\text{shorter one})^2 \times 0.52 \quad (3)$$

A slope of tumor volume-time curve, representing the growth rate, of each tumor in the treatment group (T) was obtained (days 15–27 or 8–23 for C26/control or C26/DOX tumor, respectively) and divided by that in the saline-treated (control) group (C) to give an index (T/C) for the *in vivo* therapeutic effect of each tumor-bearing mice model.

2.9. Detection of apoptotic cells within tumor tissues

PEG liposomal DOX (4 mg/kg as DOX) or saline were intravenously administered into tumor-bearing mice, when the tumor size reached about 400–500 mm^3. At 48 h after injection, tumor tissues were excised from mice and snap-frozen in acetone. Acetone-fixed 10 μm thick sections of tumor tissues were prepared with the use of cryostat (CM1850, Leica Microsystems, Wetzlar, Germany). For visualizing apoptotic cells within the tumor tissues, TUNEL staining was performed by using Tumor TACS Kit (Trevigen Inc., Gaithersburg, MD). In brief, the tumor sections were reacted with TdT enzyme for 1 h at 37 °C. Then, sections were incubated with HRP-conjugated streptavidin solution for 10 min. Peroxidase visualization was performed by DAB staining and the sections were observed under the microscope (Biozero BZ-8000, KEYENCE, Osaka).

2.10. Dual staining of vascular endothelial cells and apoptotic cells within tumor tissues

For the detection of vascular endothelial cells and apoptotic cells within the same tumor section, dual staining was performed. PEG liposomal DOX (4 mg/kg as DOX) or saline were intravenously administered into tumor-bearing mice, when the tumor size reached about 400–500 mm^3. At 48 h after injection, tumor tissues were excised from mice and processed as described in Section 2.9. For visualizing vascular endothelial cells within the tumor tissues, immunohistochemical staining for CD31 was performed. In brief, the tumor sections were incubated with rat anti-mouse CD31 antibody (550274, BD Biosciences, San Jose, CA) used at 1:10(v/v) dilution in PBS containing 5% FBS. This was followed by incubation with rhodamine isothiocyanate (RITC)-conjugated rabbit anti-rat IgG antibody (#55764, ORGANON TEKNIKA, Durham, NC). For visualizing apoptotic cells, TUNEL staining was performed by using in situ Apoptosis Detection Kit (Takara Bio Inc., Shiga, Japan) according to the recommended procedures of the Kit. In brief, the tumor sections were reacted with fluorescein isothiocyanate (FITC)-conjugated TdT enzyme for 1 h at 37 °C. The sections were observed under the fluorescence microscope (Biozero BZ-8000), and the images obtained with different filters were afterwards overlaid.

2.11. Statistical analysis

Results are expressed as the mean±S.D. of more than three experiments. Analysis of variance (ANOVA) was used to test the statistical significance of differences among groups. Statistical significance in the differences of the means was evaluated by using Student's *t*-test or Dunnett's test for the single or multiple comparisons of experimental groups, respectively.

3. Results and discussion

To confirm the acquisition of resistance of C26/DOX to DOX, the *in vitro* sensitivity of C26/DOX to DOX was evaluated. As a result, IC_{50} value of DOX to C26/DOX (40.0±6.1 μM ($n=5$), $p<0.001$) was found to be about 250 times higher than that to C26/control (0.15±0.02 μM ($n=5$)), demonstrating that C26/DOX is much more resistant to DOX than C26/control. MTT assay using PEG liposomal doxorubicin was also performed, and it was confirmed that the IC_{50} value of PEG liposomal doxorubicin (4.41±0.59 μM ($n=5$), $p<0.01$) was about 30 times larger than doxorubicin solution (0.15±0.02 μM ($n=5$)) in C26/control cells, reflecting the slow release rate of doxorubicin from PEG liposome. In the case of C26/DOX cells, IC_{50} value of PEG liposomal DOX could not be estimated since the significant cytotoxic effect was not observed even with the concentration of 100 μM as DOX. In addition, the effect of co-existence of verapamil (VER), a typical substrate of P-gp, on the *in vitro* sensitivity of C26/DOX to DOX was also evaluated. Since VER is known to be cytotoxic at high concentration [31], 10 μM VER, which did not show any cytotoxicity to either C26/DOX or C26/control, was added together with DOX, resulting in the dramatical decrease in IC_{50} value of DOX to C26/DOX (0.50±0.12 μM ($n=5$), $p<0.01$). This result suggests that the resistance of C26/DOX to DOX would be mainly ascribed to the over-expression of P-gp in C26/DOX. Then, the P-gp expression in C26/control and C26/DOX was directly evaluated by Western blotting (Fig. 1). Densitometric analysis demonstrated that P-gp expression in C26/DOX was about 10 times larger than that in C26/control, confirming that the efflux of DOX by over-expressed P-gp in C26/DOX should be mainly responsible for the resistance of C26/DOX to DOX.

Since we established the C26/DOX cells with P-gp over-expressed, the *in vivo* anti-tumor activity of DOX solution was first evaluated *in vivo*. As a result, no significant anti-tumor effect was observed even in C26/control-bearing mice with a dose of 4 mg/kg (tumor volumes on the day 19 was 110.4±7.4% of saline-treated group ($n=5$)). The reason for this result would be that DOX injected as a solution was so rapidly

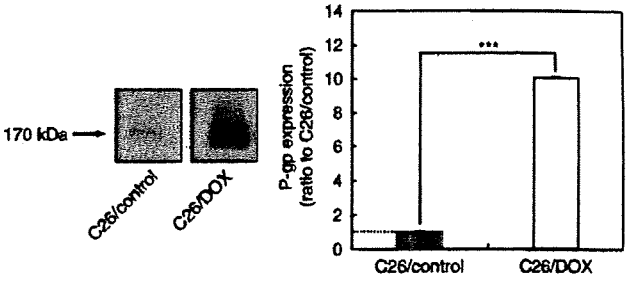

Fig. 1. Expression of P-gp in C26/control and C26/DOX. The same amount of proteins (20 μg) was loaded on each lane. Results are expressed as the mean±S.D. ($n=3$). ***$p<0.001$ compared with C26/control.

eliminated from plasma by being excreted into bile and urine and the amount of DOX distributed to tumor tissues was quite low [32,33]. Then, the EPR effect-based anti-tumor activities of PEG liposomal DOX were evaluated in both C26/control- and C26/DOX-bearing mice (Fig. 2 and Table 1). It was clearly demonstrated that the PEG liposomal DOX significantly inhibited the tumor growth in both tumor-bearing mice in a dose-dependent manner (Fig. 2). However, since the absolute tumor growth rate in the saline-treated (control) group was considerably different between C26/DOX- and C26/control-bearing mice, the index for the *in vivo* therapeutic effect (T/C), which is independent of the absolute tumor growth rate, was calculated to compare the *in vivo* efficacy of PEG liposomal DOX between these two types of tumor-bearing mice (Table 1). The T/C values, similar for both C26/contol- and C26/DOX-bearing mice in each injected dose, clearly confirmed that PEG liposomal DOX significantly suppressed the growth of not only C26/control but also C26/DOX. The reduced tumor growth rate in the tumor established by the *in vitro* long-term exposure to anti-cancer drugs was also observed by other groups [34,35] and it was speculated that the long-term exposure of tumor cells to anti-cancer drugs would affect the expression of subset of genes influencing the proliferation of tumor cells [36].

Table 1
Tumor growth rates in C26/control- or C26/DOX-bearing mice treated with PEG liposomal DOX

Dose	C26/control		C26/DOX	
	Growth rate (mm^3/day)	T/C (%)	Growth rate (mm^3/day)	T/C (%)
Saline	395.5±63.3	–	80.2±17.7	–
2 mg/kg as DOX	159.6±121.0 *	40.4	42.8±9.1*	53.4
4 mg/kg as DOX	73.9±83.9 **	18.7	15.3±12.7 **	19.1

Results are expressed as the mean±S.D. (n=5). **p<0.01; * p<0.05, compared with saline-treated group (control). The T/C index was obtained by dividing the growth rate in the treatment group (T) by that in the saline-treated group (C).

We also evaluated the survival time of tumor-bearing mice after the treatment of PEG liposomal DOX (Fig. 3). The significant extension of the mean survival time (MST) after the treatment was observed in both C26/contol- and C26/DOX-bearing mice in a dose-dependent

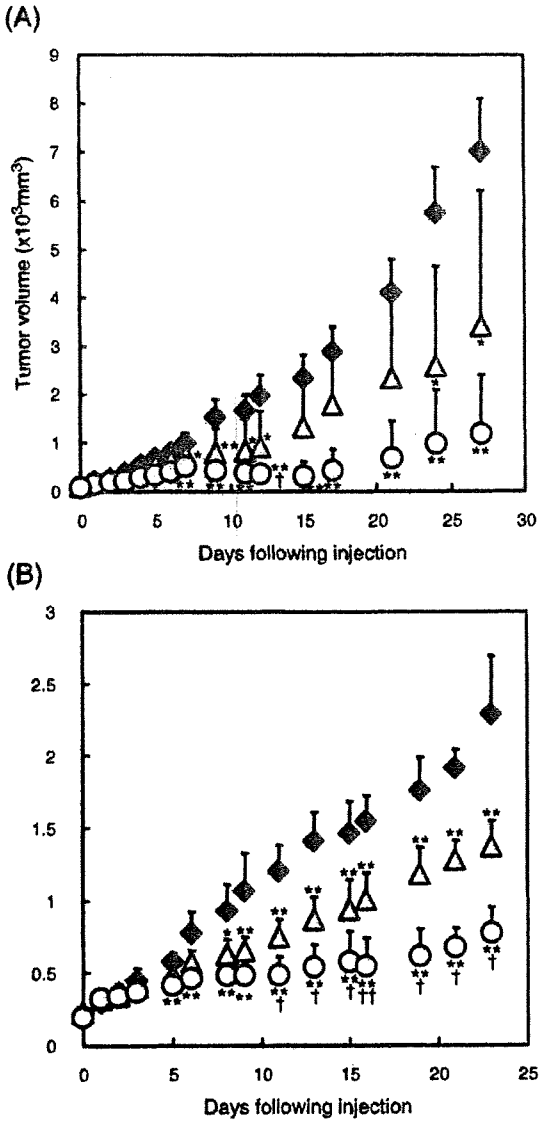

Fig. 2. Effect of PEG liposomal DOX on tumor volume in C26/control- and C26/DOX-bearing mice. (A), C26/control-bearing mice; (B), C26/DOX-bearing mice. Keys; ♦, saline; Δ, PEG liposomal DOX (2 mg/kg as DOX); ○, PEG liposomal DOX (4 mg/kg as DOX). Results are expressed as the mean±S.D. (n=5). ** p<0.01; * p<0.05, compared with saline-treated group. ††p<0.01; †p<0.05, compared with PEG liposomal DOX (2 mg/kg as DOX).

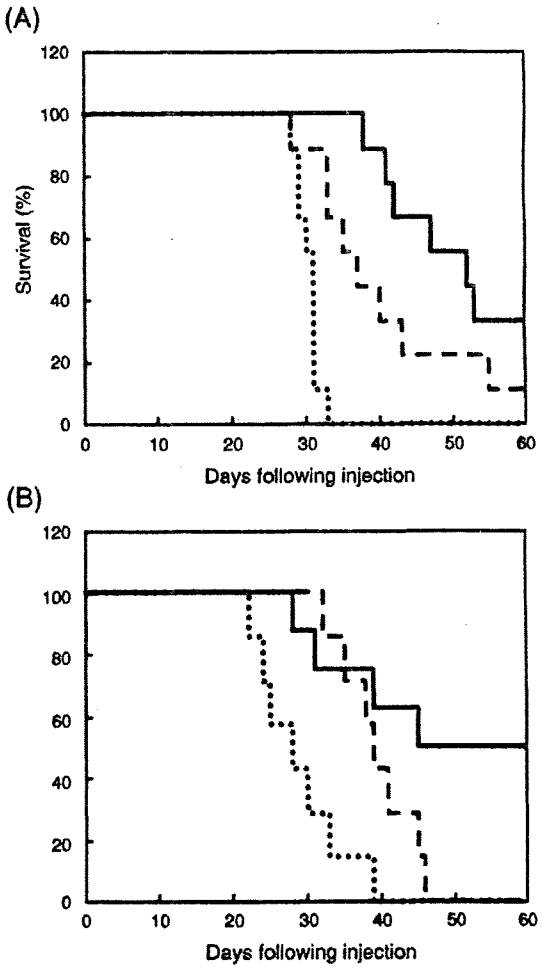

Fig. 3. Effect of PEG liposomal DOX on survival of C26/control- and C26/DOX-bearing mice. (A), C26/control-bearing mice; (B), C26/DOX-bearing mice. Keys; –, saline; —, PEG liposomal DOX (2 mg/kg as DOX); —, PEG liposomal DOX (4 mg/kg as DOX). Five mice were used in each experimental group.

manner (Table 2). T/C values expressed as MST ratio of treatment to control group were almost the same in both tumor-bearing mice in each injected dose, indicating that PEG liposomal DOX prolonged the survival time of both tumor-bearing mice to the same extent.

The results described above clearly revealed that there was a big difference in the efficacy of DOX to C26/DOX between the *in vitro* and *in vivo* studies. As possible reasons for this discrepancy between the *in vitro* and *in vivo* results, following two issues have to be taken into considerations: (i) the accumulation of PEG liposome in C26/DOX tumor might be remarkably higher than C26/control, and (ii) the expression level of P-gp in C26/DOX might go back to the normal level in the *in vivo* condition after inoculation. With regard to the former possibility, the accumulation of PEG liposome into the tumor at 48 h after intravenous administration into C26/control or C26/DOX tumor-bearing mice with the dose corresponding to 4 mg/kg DOX was evaluated and the amount was found to be similar in both tumor-bearing mice (11.6±3.2 or 11.0±2.7% of dose/g tumor in C26/control- or C26/DOX tumor-bearing mice, respectively). As for the latter possibility, Western blot analysis of tumor-homogenized samples revealed that P-gp expression within the tumor excised from C26/DOX-bearing mice was approximately 10 times larger than that from C26/control-bearing mice, demonstrating that the over-expression of P-gp would be maintained in the *in vivo* condition as well. These two additional studies clearly indicated that the amount of PEG liposomes taken up into C26/DOX was not increased and that the expression level of P-gp in C26/DOX was quite high *in vivo*. Although Goren et al. proposed the enhanced uptake of liposomes by receptor-mediated-endocytosis for overcoming P-gp-based multidrug resistance [14], this is not the case for our preparation. Furthermore, Colin de Verdière et al. suggested that the uptake of anti-tumor drug released from nanoparticles might be increased *via* passive diffusion due to the enhanced membrane permeability and/or the saturation of the efflux by P-gp [15]. However, since their proposal is based on the cell membrane damage due to the direct interaction with nanoparticles and/or their degraded components and the very rapid release of drugs from the particulates, their proposed mechanism is not our case, either. Some other reasons would, therefore, be responsible for the *in vivo* anti-tumor effects of PEG liposomal DOX observed in C26/DOX-bearing mice.

Then, the apoptosis induced within both tumors was evaluated at 48 h after intravenous administration of PEG liposomal DOX (Fig. 4), since it has been considered that the chemotherapeutic drugs cause the apoptosis of the tumor cells and it was reported that this is the case for DOX as well [35]. In the tumor excised from C26/control-bearing mice, a lot of apoptotic cells were observed throughout the tumor. On the other hand, the number of apoptotic cells within the tumor excised from C26/DOX-bearing mice was markedly smaller. These observations suggest that the resistance of C26/DOX to DOX is still maintained in the *in vivo* situation and that the *in vivo* anti-tumor effect of PEG liposomal DOX in C26/DOX-bearing mice might not be ascribed to the direct effect of DOX on tumor cells.

Solid tumors are mainly composed of tumor cells and vascular endothelial cells [37]. Endothelial cells in general are active partici-

Table 2
Mean survival time (MST) of C26/control- or C26/DOX-bearing mice treated with PEG liposomal DOX

Dose	C26/control		C26/DOX	
	MST (day)	T/C (%)	MST (day)	T/C (%)
Saline	30.3±1.5	-	28.7±5.9	-
2 mg/kg as DOX	40.4±10.7 *	133	39.4±5.1 *	133
4 mg/kg as DOX	50.3±8.7 **	166	47.9±13.9 **	167

Results are expressed as the mean±S.D. (n=5). **p<0.01; *p<0.05, compared with saline-treated group (control). The T/C index was obtained by dividing the MST of the treatment group (T) by that of the saline-treated group (C).

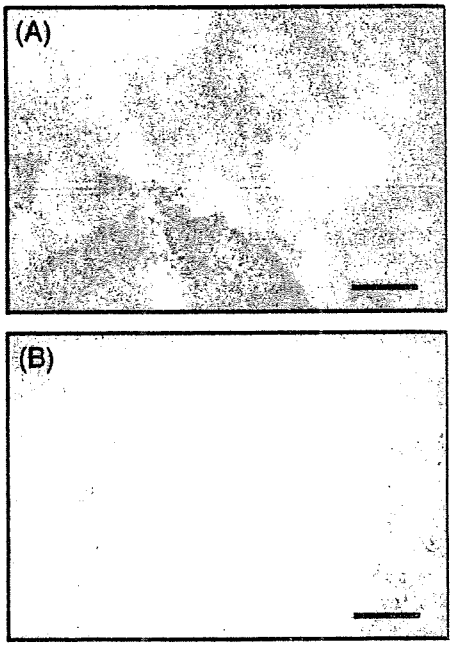

Fig. 4. Immunohistochemical staining for apoptotic cells in tumor tissues excised from C26/control- and C26/DOX-bearing mice treated with PEG liposomal DOX. (A), C26/control; (B), C26/DOX. Tumors were excised at 48 h after the treatment with PEG liposomal DOX (4 mg/kg as DOX). The cells stained with red color represent apoptotic cells. Scale bar; 200 μm. (For interpretation of the references to color in this figure legend, the reader is referred to the web version of this article.)

pants in varieties of diseases including cancer [38] and the proliferation of tumor cells are dependent on oxygen and nutrients supplied through the tumor vasculature [39]. The formation of new capillary blood vessels from existent microvessels, angiogenesis, is well known to play an important role in the growth of many types of tumors including C26 [40,41]. Therefore, we examined the possibility that the cytotoxic effects of DOX on vascular endothelial cells would be responsible for the *in vivo* anti-tumor effects of PEG liposomal DOX observed in C26/DOX-bearing mice.

At first, the sensitivity of vascular endothelial cells to DOX was evaluated by MTT assay utilizing HUVEC as a model of vascular endothelial cells [42,43]. The obtained IC_{50} value of DOX to HUVEC (0.1±0.01 μM, n=5) was approximately 1/400 of IC_{50} to C26/DOX, and this value was comparable to the IC_{50} to C26/control. This result indicates that the sensitivity of HUVEC to DOX is high and suggests that vascular endothelial cells within the tumor would be sensitive enough to DOX. Then, to directly evaluate the cytotoxic effects of DOX on vascular endothelial cells within the tumor, we performed double fluorescence immunohistochemical staining of vascular endothelial cells (red) and apoptotic cells (green) within the tumor at 48 h after intravenous administration of PEG liposomal DOX (Fig. 5). Similar to the result shown in Fig. 4, the number of apoptotic cells was much larger in the tumor excised from C26/control-bearing mice than that from C26/DOX-bearing mice. On the other hand, the distinctive area (pointed with arrows) where vascular endothelial cells (red spot) were co-localized with apoptotic cells (green dot) was more frequently observed in the tumor excised from C26/DOX-bearing mice than in C26/control tumor where such an co-localization was hardly observed. To give more quantitative evaluation, the number of apoptotic cells and % of apoptotic cells co-localized with endothelial cells were calculated from four independent microscopic fields (Fig. 6). It is worth to note that the extent of co-localization of apoptotic cells with endothelial cells was significantly higher for C26/DOX tumors (60%) than C26/control ones (20%). This result suggests

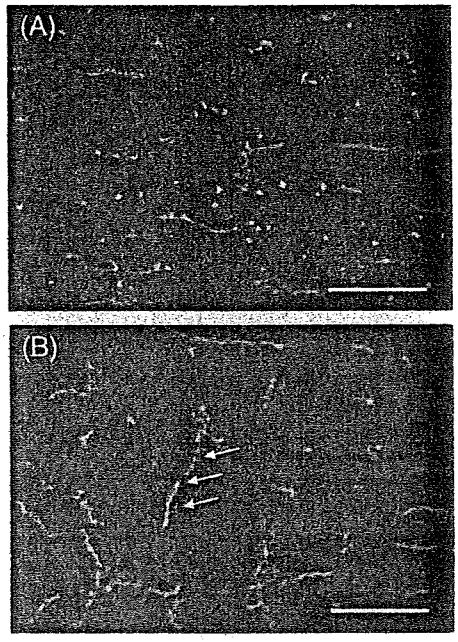

Fig. 5. Double immunohistochemical staining for apoptotic cells and endothelial cells in tumor tissues excised from C26/control- and C26/DOX-bearing mice treated with PEG liposomal DOX. (A), C26/control; (B), C26/DOX. Tumors were excised at 48 h after the treatment with PEG liposomal DOX (4 mg/kg as DOX). The cells stained with red and green color represent endothelial and apoptotic cells, respectively. White arrows (↓) point out apoptotic endothelial cells. Scale bar; 100 μm. (For interpretation of the references to color in this figure legend, the reader is referred to the web version of this article.)

that the apoptosis is caused preferentially for vascular endothelial cells in C26/DOX-bearing mice at 48 h after intravenous administration of PEG liposomal DOX. Since the number of tumor cells is recognized to be approximately 100-times larger than vascular endothelial cells in tumor tissues [37], attacking one endothelial cell is considered to lead to the death of many surrounding tumor cells [39]. It is, therefore, considered that the death of surrounding tumor cells by killing endothelial cells in C26/DOX tumors would subsequently occur at later time period.

Based on the results obtained in the present study, we propose the following mechanisms behind the *in vivo* anti-tumor effects of PEG liposomal DOX recognized in C26/DOX-bearing mice. First, the PEG liposome in the blood circulation gradually extravasated into the interstitial space of the tumor tissue due to EPR effect as reported previously [20–23]. PEG liposomes used in the present study possess the aqueous layer formed by the PEG chain and this aqueous layer interferes not only the association of serum proteins [44–47] but also the interaction with the neighboring cells [48]. Therefore, the endocytotic uptake of the PEG liposomes by tumor cells, the direct interaction between PEG liposomes and cells and the subsequent cell membrane damage are considered to hardly take place, and DOX encapsulated in the liposome must be first released into the interstitial space of the tumor to be taken up by the tumor cells via passive diffusion. This speculation was supported by the facts that PEG liposomal DOX exhibited very large value of IC_{50} in C26/control cells and that PEG liposomal DOX did not reveal the significant cytotoxic effect on C26/DOX cells as described above, because these results reflect that cytotoxic effect would be dependent on DOX slowly released out of the PEG liposome, but not DOX in liposome taken up *via* endocytosis. In the case of C26/control tumor, DOX passively taken up by C26/control would have exerted its anti-tumor activity against the tumor cells directly, leading to the apoptosis of tumor cells throughout the tumor (Figs. 4 and 5). On the other hand, in the case of C26/DOX tumor, due to the over-expressed P-gp on the surface of tumor cells (Fig. 1), DOX passively taken up by C26/DOX would have been subjected to the efflux out of the cells, which would have led to the much less apoptotic cell death in the tumor (Figs. 4, 5 and 6). Since the release of DOX from PEG liposome was very slow, it is sure that P-gp functioned effectively. Subsequently, the resultant larger amount of DOX accumulated in the interstitial space of the C26/DOX tumor tissue would have penetrated into the neighboring vascular endothelial cells. Based on MTT assay for DOX utilizing HUVEC, the vascular endothelial cells would be sensitive enough to DOX so that the vascular endothelial cells in C26/DOX tumor tissues would have been subjected to the apoptotic cell death as shown in Figs. 5(B) and 6. Subsequently, the apoptotic cell death of vascular endothelial cells would have led to the suppression of angiogenesis necessary for the tumor growth, resulting in the *in vivo* anti-tumor effect of PEG liposomal DOX in C26/DOX-bearing mice (Fig. 2 and Table 1). The direct measurement of free DOX concentration in the interstitial space of tumors will be beneficial to support the mechanisms proposed above, and this will be the subject of our further study.

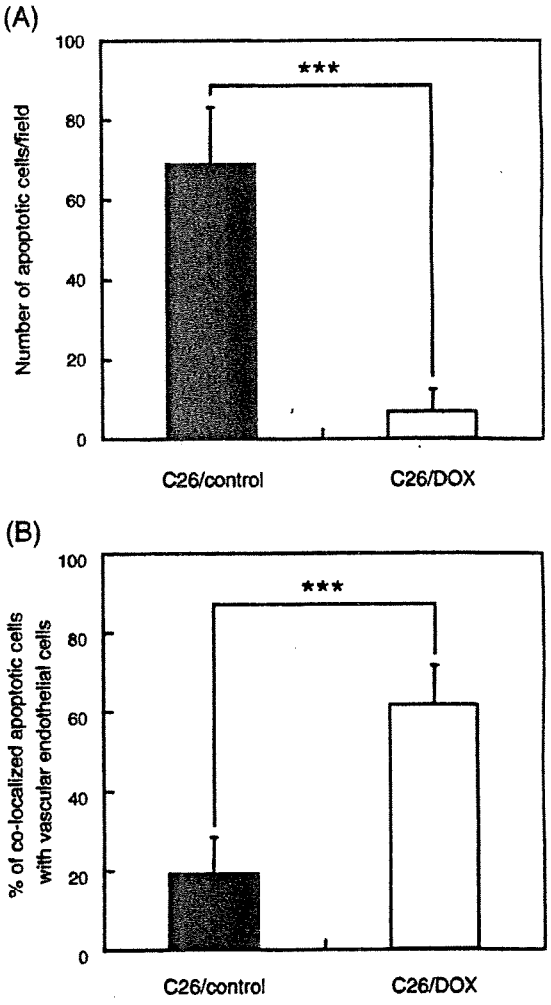

Fig. 6. Number of total apoptotic cells (A) and % of co-localized apoptotic cells with vascular endothelial cells (B) in tumor tissues excised from C26/control- and C26/DOX-bearing mice treated with PEG liposomal DOX (4 mg/kg as DOX). Apoptotic cells were counted in four independent microscopic fields. Results are expressed as the mean ± S.D. (n=4). ***p<0.001 compared with C26/control.

In conclusion, the cytotoxic effect of DOX on vascular endothelial cells in tumor tissues would be involved in the *in vivo* anti-tumor effect of PEG liposomal DOX in P-gp over-expressing tumor-bearing mice. These findings also indicate the potent efficacy of targeting of anti-angiogenic drugs to vascular endothelial cells for the cancer chemotherapy to overcome multidrug resistance.

References

[1] H.C. Chung, S.Y. Rha, J.H. Kim, J.K. Roh, J.S. Min, K.S. Lee, B.S. Kim, K.B. Lee, P-glycoprotein: the intermediate end point of drug response to induction chemotherapy in locally advanced breast cancer, Breast Cancer Res. Treat. 42 (1997) 65–72.

[2] J. Lutzky, M.B. Astor, R.N. Taub, M.A. Baker, K. Bhalla, J.E. Gervasoni, M. Rosado, V. Stewart, S. Krishna, A.A. Hindenburg, Role of glutathione and dependent enzymes in anthracycline-resistant HL60/AR cells, Cancer Res. 49 (1989) 4120–4125.

[3] R.B. Montgomery, J. Guzman, D.M. O'Rourke, W.L. Stahl, Expression of oncogenic epidermal growth factor receptor family kinases induces paclitaxel resistance and alters beta-tubulin isotype expression, J. Biol. Chem. 275 (2000) 17358–17363.

[4] Y. Miyoshi, A. Ando, Y. Takamura, T. Taguchi, Y. Tamaki, S. Noguchi, Prediction of response to docetaxel by CYP3A4 mRNA expression in breast cancer tissues, Int. J. Cancer 97 (2002) 129–132.

[5] J. Tsurutani, T. Nitta, T. Hirashima, T. Komiya, H. Uejima, H. Tada, S. Negoro, A. Tohda, M. Fukuoka, K. Nakagawa, Point mutations in the topoisomerase I gene in patients with non-small cell lung cancer treated with irinotecan, Lung Cancer 35 (2002) 299–304.

[6] F.H. Christopher, Multiple molecular mechanisms for multidrug resistance transporters, Nature 446 (2007) 479–757.

[7] E.S. Lee, K. Na, Y.H. Bae, Doxorubicin loaded pH-sensitive polymeric micelles for reversal of resistant MCF-7 tumor, J. Control. Release 103 (2005) 405–418.

[8] J.C. Wang, B.C. Goh, W.L. Lu, Q. Zhang, A. Chang, X.Y. Liu, T.M.C. Tan, H.S. Lee, In vitro cytotoxicity of Stealth liposomes co-encapsulating doxorubicin and verapamil on doxorubicin-resistant tumor cells, Biol. Pharm. Bull. 28 (2005) 822–828.

[9] M.N. Lim, N.S. Lau, K.M. Chang, C.F. Leong, Z. Zakaria, Modulating multidrug resistance gene in leukaemia cells by short interfering RNA, Singap. Med. J. 48 (2007) 932–938.

[10] J. Karwatsky, M.C. Lincoln, E. Georges, A mechanism for P-glycoprotein-mediated apoptosis as revealed by verapamil hypersensitivity, Biochemistry 42 (2003) 12163–12173.

[11] A. Breier, Z. Drobná, M. Barancík, Direct interaction between verapamil and doxorubicin causes the lack of reversal effect of verapamil on P-glycoprotein mediated resistance to doxorubicin *in vitro* using L1210/VCR cells, Neoplasma 45 (1998) 248–253.

[12] R. Krishna, M. St-Louis, L.D. Mayer, Increased intracellular drug accumulation and complete chemosensitization achieved in multidrug-resistant solid tumors by co-administering valspodar (PSC 833) with sterically stabilized liposomal doxorubicin, Int. J. Cancer 85 (2000) 131–141.

[13] T. Kobayashi, T. Ishida, Y. Okada, S. Ise, H. Harashima, H. Kiwada, Effect of transferrin receptor-targeted liposomal doxorubicin in P-glycoprotein-mediated drug resistant tumor cells, Int. J. Pharm. 329 (2007) 94–102.

[14] D. Goren, A. Horowitz, D. Tremach, M. Tarshish, S. Zalipsky, A. Gabizon, Nuclear delivery of doxorubicin via folate-targeted liposomes with bypass of multidrug-resistance efflux pump, Clin. Cancer Res. 6 (2000) 1949–1957.

[15] A. Colin de Verdière, C. Dubernet, F. Nemati, M.F. Poupon, F. Puisieux, P. Couvreur, Uptake of doxorubicin from loaded nanoparticles in multidrug-resistant leukemic murine cells, Cancer Chemother. Pharmacol. 33 (1994) 504–508.

[16] L. Barraud, P. Merle, E. Soma, L. Lefrançois, S. Guerret, M. Chevallier, C. Dubernet, P. Couvreur, C. Trépo, L. Vitvitski, Increase of doxorubicin sensitivity by doxorubicin-loading into nanoparticles for hepatocellular carcinoma cells in vitro and in vivo, J. Hepatol. 42 (2005) 736–743.

[17] S. Unezaki, K. Maruyama, J.I. Hosoda, I. Nagae, Y. Koyanagi, M. Nakata, O. Ishida, M. Iwatsuru, S. Tsuchiya, Direct measurement of the extravasation of polyethyleneglycol-coated liposomes into solid tumor tissue by in vivo fluorescence microscopy, Int. J. Pharm. 144 (1996) 11–17.

[18] A.A. Gabizon, H. Shmeeda, S. Zalipsky, Pros and cons of the liposome platform in cancer drug targeting, J. Liposome Res. 16 (2006) 175–183.

[19] J. Heyes, K. Hall, V. Tailor, R. Lenz, I. MacLachlan, Synthesis and characterization of novel poly(ethylene glycol)-lipid conjugates suitable for use in drug delivery, J. Control. Release 112 (2006) 280–290.

[20] H. Maeda, J. Wu, T. Sawa, Y. Matsumura, K. Hori, Tumor vascular permeability and the EPR effect in macromolecular therapeutics: a review, J. Control. Release 65 (2000) 271–284.

[21] A.K. Iyer, G. Khaled, J. Fang, H. Maeda, Exploiting the enhanced permeability and retention effect for tumor targeting, Drug Discov. Today 11 (2006) 812–818.

[22] D.W. Northfelt, B.J. Dezube, J.A. Thommes, B.J. Miller, M.A. Fischl, A. Friedman-Kien, L.D. Kaplan, C.D. Mond, R.D. Mamelok, D.H. Henry, Pegylated-liposomal doxorubicin versus doxorubicin, bleomycin, and vincristine in the treatment of AIDS-related Kaposi's sarcoma: Results of a randomized phase III clinical trial, J. Clin. Oncol. 16 (1998) 2445–2451.

[23] P.G. Schmidt, J.P. Adler-Moore, E.A. Forssen, R.T. Proffit, in: D.D. Lasic, D. Papahadjopoulos (Eds.), Medical Applications of Liposomes, Elsevier Science BV, New York, 1998, pp. 703–731.

[24] P.K. Working, A.D. Dayan, Pharmacological–toxicological expert report. CAELYX. (Stealth liposomal doxorubicin HCl), Human Exp. Toxicol. 15 (1996) 751–785.

[25] A. Gabizon, H. Shmeeda, Y. Barenholz, Pharmacokinetics of pegylated liposomal doxorubicin: review of animal and human studies, Clin. Pharmacokinet. 42 (2003) 419–436.

[26] K. Ogawara, K. Un, K. Minato, K. Tanaka, K. Higaki, T. Kimura, Determinants for in-vivo anti-tumor effects of PEG liposomal doxorubicin: importance of vascular permeability within tumors, Int. J. Pharm. 359 (2008) 234–240.

[27] M. Eghbali, B. Birnir, P.W. Gage, Conductance of GABAA channels activated by pentobarbitone in hippocampal neurons from newborn rats, J. Physiol. 552 (2003) 13–22.

[28] J.G. Lim, H.Y. Lee, J.E. Yun, S.P. Kim, J.W. Park, S.S. Kim, J. Han, M.J. Park, D.K. Song, Taurine block of cloned ATP-sensitive K+ channels with different sulfonylurea receptor subunits expressed in *Xenopus laevis* oocytes, Biochem. Pharmacol. 68 (2004) 901–910.

[29] K. Yamaoka, Y. Tanigawa, H. Tanaka, Y. Uno, A pharmacokinetic analysis program (MULTI) for microcomputer, J. Pharmacobio-Dyn. 4 (1981) 879–885.

[30] G. Haran, R. Cohen, L.K. Bar, Y. Barenholz, Transmembrane ammonium sulfate gradient in liposomes produce efficient and stable entrapment of amphipathic weak bases, Biochim. Biophys. Acta 1151 (1993) 201–215.

[31] R. Sadasivan, R. Morgan, C. Fabian, R. Stephens, Reversal of multidrug resistance in HL-60 cells by verapamil and liposome-encapsulated doxorubicin, Cancer Lett. 57 (1991) 165–171.

[32] A.A. Gabizon, M. Chemla, D. Tzemach, A.T. Horowitz, D. Goren, Liposome longevity and stability in circulation: effects on the *in vivo* delivery to tumors and therapeutic efficacy of encapsulated anthracyclines, J. Drug Target. 3 (1996) 391–398.

[33] L.D. Mayer, L.C. Tai, D.S. Ko, D. Masin, R.S. Ginsberg, P.R. Cullis, M.B. Bally, Influence of vesicle size, lipid composition, and drug-to-lipid ratio on the biological activity of liposomal doxorubicin in mice, Cancer Res. 49 (1989) 5922–5930.

[34] J. Qi, S. Wang, G. Liu, H. Peng, J. Wang, Z. Zhu, C. Yang, Pyronaridine, a novel modulator of P-glycoprotein-mediated multidrug resistance in tumor cells *in vitro* and *in vivo*, Biochem. Biophys. Res. Commun. 319 (2004) 1124–1131.

[35] K. Shimizu, T. Asai, C. Fuse, Y. Sadzuka, T. Sonobe, K. Ogino, T. Taki, T. Tanaka, N. Oku, Applicability of anti-neovascular therapy to drug-resistant tumor: suppression of drug-resistant P388 tumor growth with neovessel-targeted liposomal adriamycin, Int. J. Pharm. 296 (2005) 133–141.

[36] M. Jakobisiak, J. Golab, Potential antitumor effects of statins, Int. J. Oncol. 23 (2003) 1055–1069.

[37] J. Folkman, Angiogenesis in cancer, vascular, rheumatoid and other disease, Nat. Med. 1 (1995) 27–31.

[38] P. Carmeliet, R.K. Jain, Angiogenesis in cancer and other diseases, Nature 14 (2000) 249–257.

[39] G. Molema, D.L. Meijer, L.F. de Leij, Tumor vasculature targeted therapies: getting the players organized, Biochem. Pharmacol. 55 (1998) 1939–1945.

[40] N.M. Pandya, N.S. Dhalla, D.D. Santani, Angiogenesis: a new target for future therapy, Vasc. Pharmacol. 44 (2006) 265–274.

[41] R.M. Schiffelers, J.M. Metselaar, M.H. Fens, A.P. Janssen, G. Molema, G. Storm, Liposome-encapsulated prednisolone phosphate inhibits growth of established tumors in mice, Neoplasia 7 (2005) 118–127.

[42] K. Ogawara, M.G. Rots, R.J. Kok, H.E. Moorlag, A.M. Van Loenen, D.K. Meijer, H.J. Haisma, G. Molema, A novel strategy to modify adenovirus tropism and enhance transgene delivery to activated vascular endothelial cells in vitro and in vivo, Hum. Gene Ther. 15 (2004) 433–443.

[43] J.M. Kuldo, J. Westra, S.A. Asgeirsdóttir, R.J. Kok, K. Oosterhuis, M.G. Rots, J.P. Schouten, P.C. Limburg, G. Molema, Differential effects of NF-κB and p38 MAPK inhibitors and combinations thereof on TNF-α- and IL-1β-induced proinflammatory status of endothelial cells *in vitro*, Am. J. Physiol. Cell Physiol. 289 (2005) C1229–1239.

[44] N. Oku, Y. Namba, Glucuronate-modified, long-circulating liposomes for the delivery of anticancer agents, Methods Enzymol. 391 (2005) 145–162.

[45] Y. Sadzuka, I. Sugiyama, T. Tsuruda, T. Sonobe, Characterization and cytotoxicity of mixed polyethyleneglycol modified liposomes containing doxorubicin, Int. J. Pharm. 312 (2006) 83–89.

[46] T. Shehata, K. Ogawara, K. Higaki, T. Kimura, Prolongation of residence time of liposome by surface-modification with mixture of hydrophilic polymers, Int. J. Pharm. 359 (2008) 272–279.

[47] J. Yokoe, S. Sakuragi, K. Yamamoto, T. Teragaki, K. Ogawara, K. Higaki, N. Katayama, T. Kai, M. Sato, T. Kimura, Albumin-conjugated PEG liposome enhances tumor distribution of liposomal doxorubicin in rats, Int. J. Pharm. 353 (2008) 28–34.

[48] H. Hatakeyama, H. Akita, K. Kogure, M. Oishi, Y. Nagasaki, Y. Kihira, M. Ueno, H. Kobayashi, H. Kikuchi, H. Harashima, Development of a novel systemic gene delivery system for cancer therapy with a tumor-specific cleavable PEG-lipid, Gene Ther. 14 (2007) 68–77.

Heterogeneous Polymerization with Polyaspartate Macromonomer Having Vinyl Pendant Groups. I. Synthesis of Macromonomer and Dispersion Copolymerization of Styrene

KEISUKE TOMITA, TSUTOMU ONO

Department of Material and Energy Science, Graduate School of Environmental Science, Okayama University, 3-1-1 Tsushima-Naka, Okayama 700-8530, Japan

Received 4 September 2008; accepted 8 November 2008
DOI: 10.1002/pola.23192
Published online in Wiley InterScience (www.interscience.wiley.com).

ABSTRACT: Sodium polyaspartate (PAspNa) derivatives with vinylbenzyl pendant groups (VBA-PAspNa) were synthesized by reaction of poly(succinimide) (PSI) and vinylbenzylamine (VBA), and hydrolysis by sodium hydroxide (NaOH) solution. VBA-PAspNa is a macromonomer with multiple vinyl groups in the side chain. Submicron sized polymeric particles were prepared by dispersion copolymerization of styrene with VBA-PAspNa in a mixture of ethanol and water. Particle diameter decreased with increasing concentration and vinyl group fraction of VBA-PAspNa. When compared with the particle diameter prepared using PAspNa or benzylamine-modified PAspNa (BA-PAspNa) as a dispersion stabilizer without vinyl groups, the particles prepared with VBA-PAspNa were an order smaller than those prepared with PAspNa or BA-PAspNa. The particles after refinement show an adequate negative ζ-potential. From this result, we clarified the presence of PAspNa chains anchored onto the particle surface. ©2008 Wiley Periodicals, Inc. J Polym Sci Part A: Polym Chem 47: 762–770, 2009
Keywords: colloids; dispersion polymerization; macromonomers; particle; polyaspartate

INTRODUCTION

Recently, particles with specific functions have been widely developed. Functional particles have great potential for a lot of applications such as paints, pigments, cosmetics, adhesives, catalyst carriers, technology materials, electrical parts, and drug delivery carriers. Because the characteristics of the particles are mainly based on the surface, particles coated with functional groups have been remarkably investigated.

Heterogeneous polymerization processes, emulsion copolymerization or dispersion copolymerization using a macromonomer, are a suitable method to create functional particles. In these polymerization systems, a macromonomer acts not only as a comonomer but as a dispersion stabilizer. Thus, the particles obtained have high stability and functionality due to the presence of macromonomers immobilized on the particle surface. Macromonomers used for heterogeneous polymerization are based on poly(2-oxazoline),[1,2] poly(ethylene oxide) (PEO),[3–16] poly(*N*-vinylpyrrolidone),[17] poly(methacrylic acid),[18,19] poly(acrylic

Correspondence to: T. Ono (E-mail: tono@cc.okayama-u.ac.jp)
Journal of Polymer Science: Part A: Polymer Chemistry, Vol. 47, 762–770 (2009)

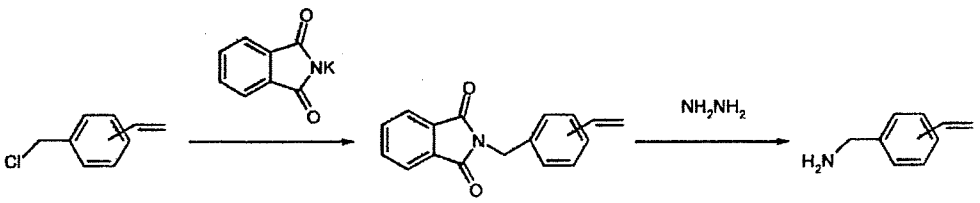

Scheme 1. Synthesis of VBA.

acid),[20] poly(4-vinyl-*N*-*n*-butylpyridonium bromide),[21] and poly(2-(dimethylamino)ethylmethacrylate.[22] Especially, almost all studies used the macromonomer based on PEO because of its high solubility in various solvents. However, the functionalization of PEO chains is difficult owing to the chemical stability of ethylene oxide units.

Sodium polyaspartate (PAspNa), a hydrophilic biodegradable polymer, can easily accept the introduction of functional groups into the side chains. PAspNa is derived from poly(succinimide) (PSI), product from the polycondensation of L-aspartic acid, by hydrolysis with sodium hydroxide.[23] PSI reacts with various amine compounds without any coupling agent. Therefore, PAspNa derivatives with various functional pendant groups are easily designed.[23–26]

A PAspNa derivative with vinylbenzyl pendant groups (VBA-PAspNa) is obtained by introduction of vinylbenzylamine (VBA) into PSI. VBA-PAspNa was used as a macromonomer in dispersion polymerization, resulting in the PAspNa-anchored particles. Because a PAspNa chain is available for the introduction of functional groups into the side chain, this method is promising to prepare polymeric particles with functional polymer chains on the surface.

In general, a macromonomer has one or two vinyl end groups in the chain. However, VBA-PAspNa has multiple vinyl groups in the side chain. We can expect that the molar ratio of vinylbenzyl group units in the polymer chain, vinyl group fraction, will affect the polymerization mechanism. Since there was no report about dispersion copolymerization with a macromonomer with multiple vinyl groups in the side chain, we focus on the dispersion copolymerization using VBA-PAspNa.

In this study, VBA-PAspNa with different vinyl group fractions were synthesized and used as a macromonomer in dispersion copolymerization of styrene in a mixture of ethanol and water. The effects of concentration, vinyl group fraction, and molecular weight of VBA-PAspNa on the polystyrene particle diameter were investigated. To clarify the effect of vinylbenzyl pendant groups in VBA-PAspNa on the particle formation, the diameter of particles obtained by using VBA-PAspNa was compared with that obtained by using PAspNa or a benzylamine-modified PAspNa derivative (BA-PAspNa), a dispersion stabilizer without any vinyl groups. The surface property of the particles was estimated by ζ-potential measurement.

EXPERIMENTAL

Material

Vinylbenzyl chloride (a mixture of 3- and 4-isomers) was obtained from Aldrich. Other materials were obtained from Wako Pure Chemical Industries. *N,N*-dimethylformamide (DMF) was purified by distillation under reduced pressure and was dehydrated by adding dried molecular sieves. Styrene was purified by distillation under reduced pressure. 2,2′-Azobisisobutyronitrile (AIBN) was purified by recrystallization from ethanol. 4-*t*-Butylpyrocatechol was used without further purification. Water was purified by a Millipore Milli-Q purification system.

Synthesis of VBA (Scheme 1)

The synthesis of VBA, an introducing reagent to PSI chains, was carried out using the following two steps:

Step 1: Synthesis of *N*-vinylbenzylphtalimide

40.6 g of potassium phthalimide and 30.8 g of vinylbenzyl chloride were dissolved in dried DMF 100 g, the mixture was poured into a reactor that was equipped with a reflux condenser. The reactor was purged with nitrogen gas for 5 min, heated at temperature of 323 K for 5 h. After the reaction, the reaction mixture was added into 500 mL of chloroform, and then was washed with water

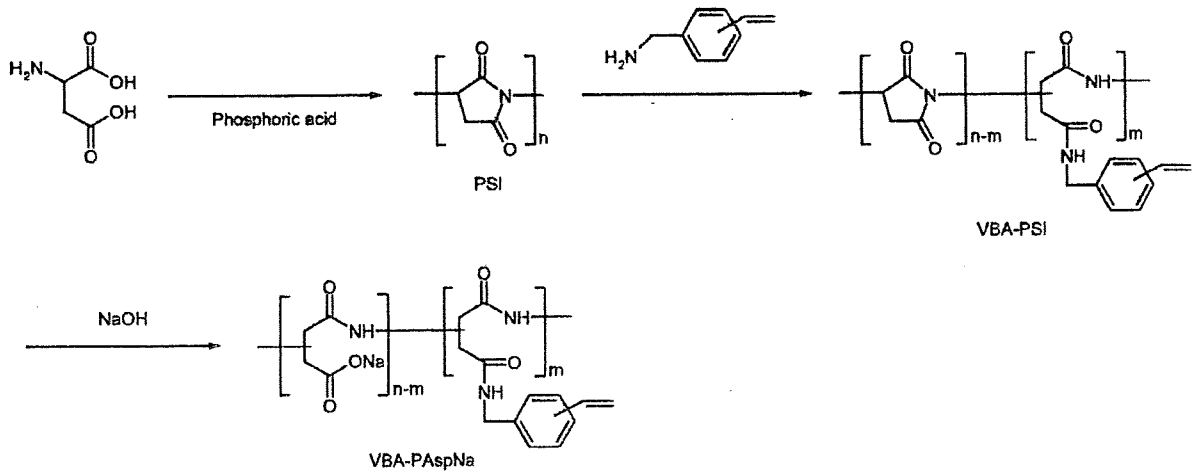

Scheme 2. Synthesis of VBA-PAspNa.

(300 mL × 3), 0.2 N sodium hydroxide (NaOH) solution (120 mL), and water (120 mL). Chloroform was removed under reduced pressure. The mixture was precipitated into 200 mL of methanol and filtered. The precipitate was dried in a vacuum to give *N*-vinylbenzylphthalimide (48.1 g, 83%).

^{1}H NMR (300 MHz, $CDCl_3$, ppm): 4.83 (m, 2H, CH_2), 5.23 (m, 1H,=CH), 5.73 (m, 1H, =CH), 6.68 (m, 1H, =CH), 7.34 (m, 4H, Ar), 7.71–7.84 (m, 4H, Ar (Pht)).

Step 2: Synthesis of Vinylbenzylamine

26.3 g of *N*-vinylbenzylphthalimide was dissolved in 50 mL of ethanol in the reactor with reflux condenser. The mixture was stirred at reflux temperature (353 K) for 1 h. 10 mL of ethanol solution dissolving 6.2 g hydrazine monohydrate was slowly added to the stirred mixture. 180 mL of 15 wt % potassium hydroxide (KOH) solution was also added to the mixture, and was stirred for 3 h. After cooling the reaction mixture, it was filtered to remove unreacted material. The filtrate was mixed with 500 mL of diethyl ether and the organic phase was washed with 2 wt % KOH solution (50 mL ×4). The organic layer was dried with anhydrous potassium carbonate. The solvent was removed under reduced pressure to yield VBA (9.3 g, 61%).

^{1}H NMR (300 MHz, $CDCl_3$, ppm): 1.62 (s, 2H, NH_2), 3.85 (m, 2H, CH_2), 5.23 (m, 1H, =CH), 5.73 (m, 1H, =CH), 6.71 (q, 1H, =CH), 7.30 (m, 4H, Ar).

Synthesis of VBA-PAspNa (Scheme 2)

The synthesis of VBA-PAspNa was carried out using the following three steps:

Step 1: Synthesis of PSI

PSI was synthesized by the thermal bulk polycondensation of L-aspartic acid using phosphoric acid as a catalyst according to the method described by Neri et al.[23]

Step 2: Synthesis of VBA Modified PSI (VBA-PSI)

A typical procedure for the synthesis of VBA-modified PSI (VBA-PSI) is as follows: 11.0 g of PSI was dissolved in 60 g of dry DMF. The mixture was replaced in a flask equipped with a reflux condenser. The flask was purged with nitrogen gas for 5 min and heated at 333 K. 1.52 g of VBA was added to the mixture and was stirred for 4 h. The reaction mixture was concentrated under reduced pressure and precipitated into water. The precipitate was washed with methanol. The resultant polymer was dried in vacuum to obtain the VBA-PSI (11.8 g, 94%).

Step 3: Synthesis of VBA-PAspNa

A typical procedure for the synthesis of VBA-modified PAspNa (VBA-PAspNa) is as follows: 11.0 g of VBA-PSI was dispersed in 200 mL of water, and 1 N NaOH solution was added dropwise so as not to exceed pH 10 in the solution. The solution was then neutralized by 1 N hydrochloric acid solution and concentrated under reduced pressure. The solution was precipitated into methanol. The precipitate was dried under vacuum to obtain VBA-PAspNa (12.7 g, 84%).

Dispersion Copolymerization

Dispersion copolymerization was carried out in a reactor equipped with a reflux condenser and a magnetic stirrer that was placed in an oil bath equipped with a temperature control. A typical procedure for dispersion copolymerization of styrene with VBA-PAspNa is presented below: 0.107 g of AIBN and 1.34 g of styrene were dissolved in 27 mL of ethanol and was added into 18 mL of aqueous solution containing of 0.10 g VBA-PAspNa. The mixture was polymerized in the reactor at 343 K for 6 h under nitrogen atmosphere. The resultant particles were refined by three centrifugating washes with water.

Measurements and Characterization

^{1}H NMR spectra were measured using a NMR spectrometer (JEOL, AL300 SC-NMR). Molecular weights of PSI were determined by a gel permeation chromatography (GPC, TOSOH HLC-8120 GPC system) using polystyrene standards with DMF as an eluant. The flow rate and the column temperature were 0.6 mL/min and 313 K, respectively. The particle diameter and the diameter distribution were determined by scanning electron microscopy (SEM, Hitachi *S*-4700). The number-average particle diameter was obtained by counting 200 particles in SEM photographs. Coefficient of variation (CV) of the particle diameter was calculated from the following equation:

$$\mathrm{CV}(\%) = \frac{\text{Standard derivation } (\mu\text{m})}{\text{Number-average particle diameter } (\mu\text{m})} \times 100 \quad (1)$$

Styrene monomer conversion was calculated from the unreacted styrene monomer concentration, which is measured by high-performance liquid chromatography. Small amount of samples withdrawn at different polymerization intervals were added to methanol with 4-*t*-butylpyrocatechol to terminate polymerization. These solutions were centrifuged at 30,000 rpm for 15 min to remove the particles. Unreacted styrene concentration in the supernatant was measured by high-performance liquid chromatography (TOSOH SC-8010 system) with a UV–vis detector (UV-8010, $\lambda = 254$ nm) with the mixture of methanol/water = 7/3 (vol/vol) as an eluant. The column was a TSK-Gel ODS-80Ts QA (150 × 4.6 mm^2, TOSOH). The flow rate and the column temperature were 0.8 mL/min and 313 K, respectively. Particle number was calculated on the basis of the particle diameter and styrene monomer conversion. ζ-Potential of the particles was measured by using an electrophoretic light scattering spectrophotometer (Otuka Electronics ELS-6000).

RESULTS AND DISCUSSION

Synthesis and Characterization of PAspNa Macromonomers

In this study, the feed molecular fractions of VBA to succinimide unit of PSI were 5, 10, 15, and 20 mol %. Weight-average molecular weight (M_w) of PSI used for the synthesis of VBA-PAspNa were between ~6000 and ~30,000.

The typical ^{1}H NMR spectra of VBA-PSI and VBA-PAspNa are shown in Figure 1. Hydrolysis of PSI units was confirmed by decrease of the peak at 5.3 ppm for a methine proton of a succinimide unit and the appearance of the peaks at 4.5 and 4.7 ppm for methine protons of aspartic acid units. Though the hydrolysis of succinimide units was completed, the peak at 4.5 ppm remained. This peak is based on the *trans*-vinyl proton in the side chain.

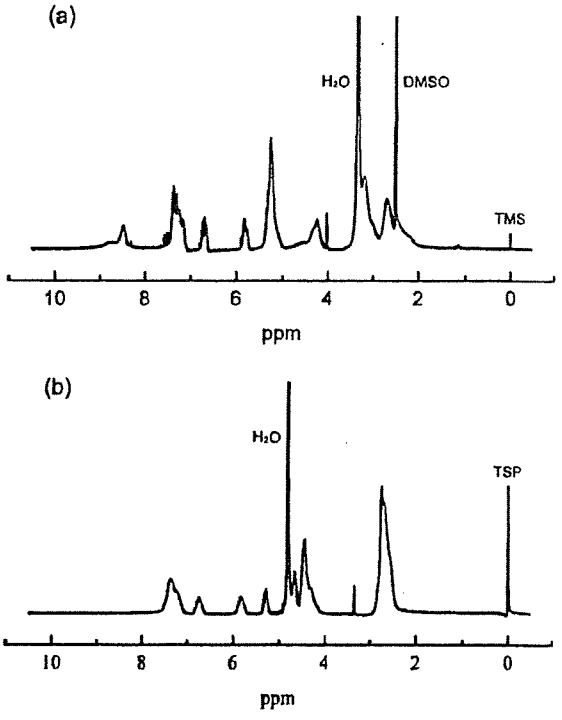

Figure 1. ^{1}H NMR spectra of (a) VBA-PSI in DMSO-d_6 and (b) VBA-PAspNa in D_2O.

Table 1. Conditions of Synthesis and Vinyl Group Fraction of VBA-PaspNa

Sample	PSI		VBA/SI[b] (mol %)	Vinyl Group Fraction[c] (mol %)
	M_w[a]	M_w/M_n[a]		
VBA-5-PAspNa-30k	3.0×10^4	2.9	5	5
VBA-9-PAspNa-6k	6.0×10^3	3.5	10	9
VBA-9-PAspNa-31k	3.1×10^4	2.3	10	9
VBA-10-PAspNa-30k	3.0×10^4	2.9	11	10
VBA-13-PAspNa-31k	3.1×10^4	2.3	15	13
VBA-18-PAspNa-31k	3.1×10^4	2.3	20	18

[a] Measured by GPC.
[b] Molecular fraction of VBA to succinimide unit of PSI.
[c] Determined by ^{1}H NMR spectrum.

Vinyl group fraction was calculated by integration values of a vinyl proton peak at 5.8 ppm and a methine proton peak of a succinimide unit at 5.3 ppm in the ^{1}H NMR spectrum of VBA-PSI. Table 1 shows the vinyl group fraction of VBA-PAspNa. The feed mole ratios of VBA and succinimide units to PSI mostly corresponded to the vinyl group fraction calculated by a ^{1}H NMR spectrum. The feed mole ratios of VBA and succinimide units to PSI can control the vinyl group fraction in VBA-PAspNa.

Preparation of Polymeric Particles

Figure 2 shows the time courses of styrene monomer conversion, particle diameter, CV, and particle number in dispersion copolymerization of styrene with VBA-PAspNa in a mixture of ethanol and water. The conversion approached approximately constant (>90%) within 3 h. Particle diameter also gradually increased with progress of polymerization time. These show quite similar tendency. Particle number was stabilized at a constant value, during the polymerization, after its fast increase. The CV of particle diameter increased up to 45 min, then became almost constant. From these results, we consider that this polymerization mechanism is as follows: Particle nucleation and aggregation has occurred in the initial stage to form stable particles. As the nucleation and aggregation proceed simultaneously, the CV value increases during this period. After this stage, the propagation of particles is developed by capturing monomers and/or oligomers from the continuous phase.

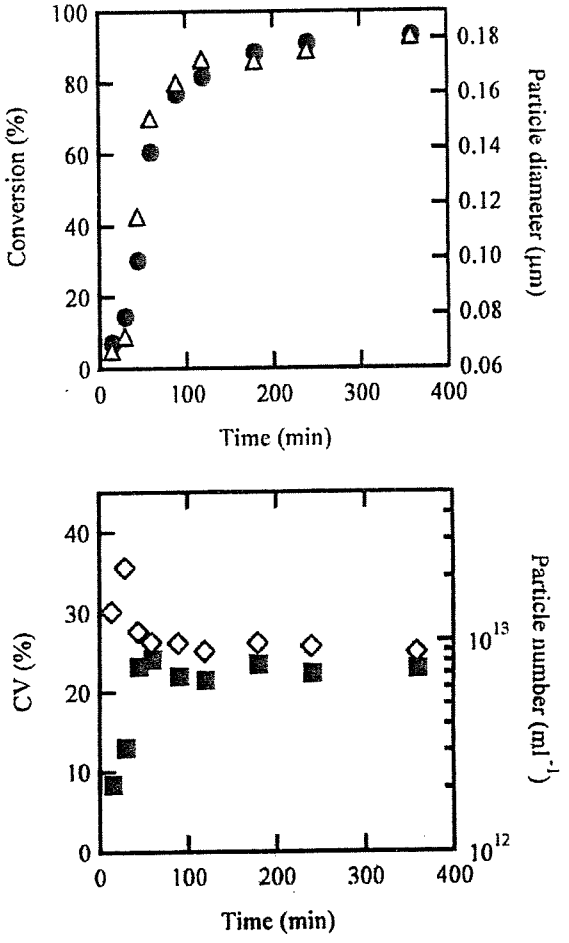

Figure 2. Time courses of styrene monomer conversion (●), particle diameter (△), CV (■), and particle number (◇) in dispersion copolymerization of styrene with VBA-10-PAspNa-30k, [VBA-PAspNa] = 1.11 g/L.

Table 2. Particle Diameter and CV of Particle Prepared by Dispersion Copolymerization with VBA-PaspNa

Macromonomer	Concentration (g/L)	dp^a (μm)	CV^b (%)
VBA-9-PAspNa-31k	0.22	0.277	16.7
	2.22	0.177	24.4
	4.44	0.157	21.9
VBA-9-PAspNa-6k	2.22	0.173	25.4
VBA-5-PAspNa-30k	2.22	0.208	22.0
VBA-13-PAspNa-31k	2.22	0.168	16.0
VBA-18-PAspNa-31k	2.22	0.150	20.2

[a] Number-average particle diameter determined by SEM.
[b] Coefficient of variation.

Particle diameter and CV of the particles prepared with various concentrations, vinyl group fractions, and molecular weight of VBA-PAspNa are shown in Table 2. In spite of low macromonomer concentration (<1 g/L), stable particles with submicron size were obtained. The particles prepared in this study were smaller than those prepared with PEO macromonomer under similar conditions.[15] The particle diameter distribution was broad irrespective of the concentration, the vinyl group fraction, and molecular weight of the VBA-PAspNa.

From the results of Table 2, particle diameter decreased with increasing vinyl group fraction of the VBA-PAspNa. In the system of dispersion copolymerization with macromonomer, homopolymers and graft copolymers (polymerized chains of monomers and macromonomers) were supposed to be formed. The aggregation of homopolymers and graft copolymers results in the particle nuclei. When the concentration or the vinyl group fraction of VBA-PAspNa is high, the copolymerization of VBA-PAspNa and styrene is enhanced, and the influence of graft copolymers is also increased. Thus, the aggregation of particle nuclei is prevented by graft copolymers, resulting in the increase of the particle number formed at the beginning of polymerization. Eventually, the smaller particles are obtained.

The molecular weight of VBA-PAspNa did not significantly affect the particle diameter. A particle diameter is determined by the surface area occupied by the macromonomer chains.[5] Because VBA-PAspNa is a random copolymer bearing vinylbenzyl groups, VBA-PAspNa is expected to attach at multiple sites on the particle surface. That is why the amount of grafted VBA-PAspNa onto the particle surface is independent of the molecular weight of VBA-PAspNa. Therefore, surface area per unit weight of macromonomer was not changed even though the macromonomer chain length was increased.

Effect of VBA-PAspNa Concentration

Dispersion stabilizer concentration is a representative parameter affecting particle diameter in dispersion polymerization. The effect of VBA-PAspNa on the particle diameter is shown in Figure 3. The particle diameter decreased with increasing VBA-PAspNa concentration and is expressed as the following equation:

$$d_p = [\text{VBA} - \text{PAspNA}]^{-0.19}$$

It was found that the vinyl group fraction of VBA-PAspNa did not affect the dependence of macromonomer concentration. The value of exponent is much smaller than that of a theoretical value for dispersion copolymerization with macromonomer, −0.50, predicted by Kawaguchi et al.[5] However, several values of exponent between −0.30 and −0.93 were obtained from experimental results on the dispersion copolymerization of styrene with PEO macromonomer.[8,9,11,15] It may depend on the polymerization condition. The dispersion copolymerization of methyl methacrylate

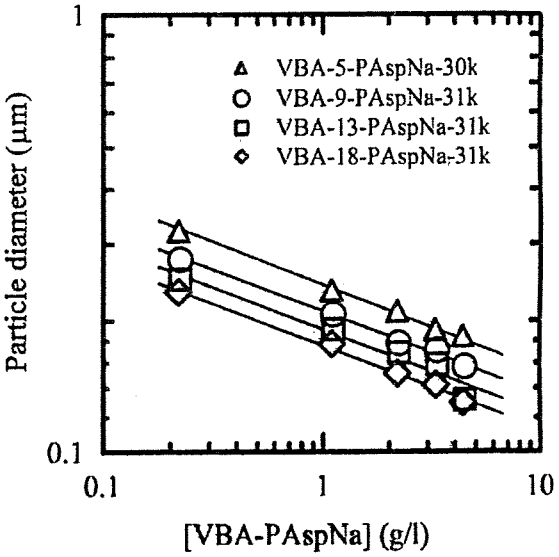

Figure 3. Effect of VBA-PAspNa concentration on particle diameter of the particles prepared by dispersion copolymerization of styrene with VBA-PAspNa.

Table 3. Chemical Structures and Composition of Dispersion Stabilizers Based on PAspNa

Dispersion Stabilizer	Structure	M_w of PSI[a]	Pendant Group Fraction[b] (mol %)
PAspNa (Homopolymer)	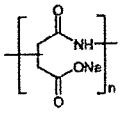	4.3×10^4	–
BA-PAspNa (Amphiphilic copolymer)	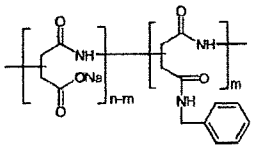	3.1×10^4	10
VBA-PAspNa (Macromonomer)	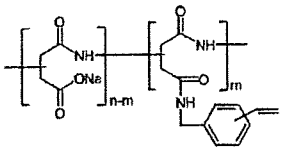	3.1×10^4	9

[a] Measured by GPC.
[b] Determined by ^{1}H-NMR spectrum.

with poly(methacrylic acid) macromonomer showed the different dependencies of macromonomer concentration on particle diameter with varying polarity of the medium.[19] When the polymerization was carried out in the mixture of ethanol and water (5:5), the particle diameter was constant regardless of macromonomer concentration. On the other hand, in the case of the polymerization in the mixture of ethanol and water (7:3), the particle diameter increased with increasing macromonomer concentration. These results are interpreted by the solubility decrease of macromonomer in a solvent. This implied that the dependence of macromonomer concentration on the particle diameter was influenced by the solubility of macromonomer in a solvent. Since ethanol is a poor solvent for PAspNa, the solubility of VBA-PAspNa in a mixture of ethanol and water was not sufficient. This may result in a low value of exponent in dispersion copolymerization with VBA-PAspNa.

Effect of Chemical Structure of Dispersion Stabilizers

In general, dispersion stabilizers used in dispersion polymerization are classified as follows: (a) homopolymers, (b) amphiphilic copolymers, and (c) macromonomers. To confirm the effect of vinyl groups of a dispersion stabilizer, the diameter of particles prepared using PAspNa macromonomer (VBA-PAspNa) was compared with that using PAspNa homopolymer (PAspNa) and a PAspNa derivative containing benzyl pendant groups (BA-PAspNa). Chemical structures and composition of dispersion stabilizers used in this section are summarized in Table 3.

The comparison of dispersion stabilizers to the particle diameter is shown in Figure 4. Micron-sized particles were prepared in dispersion polymerization using PAspNa-43k[27] or BA-10-PAspNa-31k as a dispersion stabilizer. The diameter of particles prepared using BA-10-PAspNa-31k was much smaller than that using PAspNa-43k. When low concentrations of BA-10-PAspNa-31k ([BA-PAspNa] = 0.22–1.1 g/L) was used, the particles with bimodal particle diameter distribution were obtained. On the other hand, the diameter of particles using VBA-9-PAspNa-31k was decreased to submicron size, and we did not observe bimodal particle diameter distribution.

The small particles obtained using BA-10-PAspNa-31k were due to the hydrophobicity of benzyl groups in the side chain involving in the

adsorption of BA-10-PAspNa-31k onto the particle nuclei. However, VBA-9-PAspNa-31k gave much smaller particles than that obtained by BA-10-PAspNa-31k. This comparison result indicated that an important factor for particle stabilization is not hydrophobicity but reactivity of vinylbenzyl pendant group.

Characterization of Particle Surface

Macromonomers copolymerize with monomers and bind to the particles. The presence of macromonomer chains on the surface significantly affect the properties, such as a dispersion stability, of resultant particles. To confirm the presence of macromonomer on the surface of particles prepared with VBA-5-PAspNa-30k, ζ-potential of the particles was measured. The surface has negative charge from the carboxylate group of PAspNa chains, if the particles surface is covered with macromonomers. The results of ζ-potential measurement of the particles prepared with different VBA-5-PAspNa-30k concentrations is shown in Figure 5. As shown in this figure, the particles after refinement had a high negative charge on the surface. This indicated that PAspNa chains having a negative charge were fixed onto the surface of particles. Consequently, VBA-PAspNa is bound to the particle surface and gives dispersion stability to the particles through dispersion copolymerization method. Moreover, since PAspNa can be modified with various functional pendant groups, it will be a promising way to prepare functional polymeric particles.

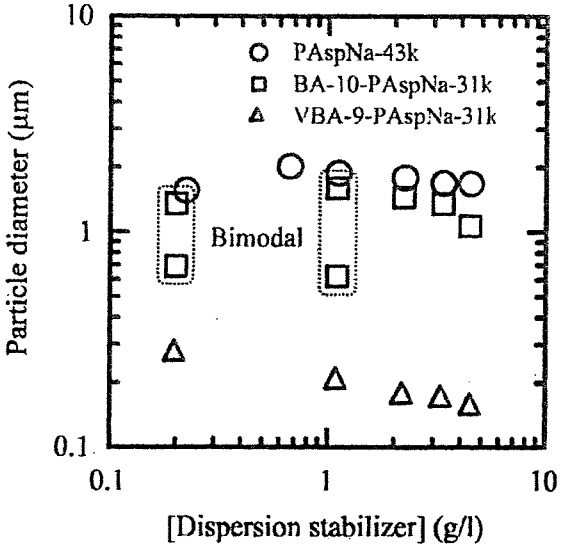

Figure 4. Comparison results of particle diameter with different type of dispersion stabilizers.

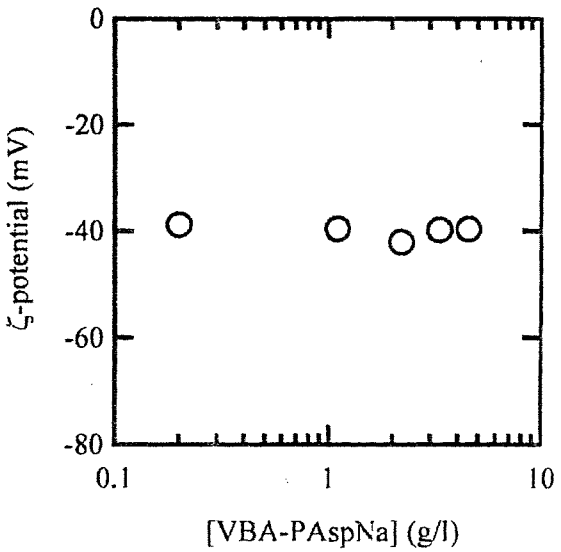

Figure 5. ζ-Potential of the particles prepared by dispersion copolymerization with different VBA-5-PAspNa-30k concentrations.

CONCLUSIONS

PAspNa macromonomers having vinylbenzyl pendant groups (VBA-PAspNa) were synthesized. VBA-PAspNa with different vinyl group fraction were synthesized by changing feed VBA. Submicron sized polymeric particles were prepared by dispersion copolymerization of styrene with VBA-PAspNa in a mixture of ethanol and water. In the present polymerization system, styrene monomer conversion and particle diameter increased with the progress of polymerization, they showed similar tendency, and particle number was constant in 1 h. The particle diameter decreased with increasing concentration and vinyl group fraction of VBA-PAspNa. Comparing the results of dispersion polymerization using PAspNa or benzylamine-modified PAspNa derivative, it was found that VBA-PAspNa is an effective stabilizer in dispersion polymerization in a mixture of ethanol and water. The presence of PAspNa chains anchored onto the particle surface was confirmed by ζ-potential measurement. In PAspNa, functional groups can be easily introduced into the side chain; thus the present method is a process for preparation of polymeric particles with various functional polymer chains on the surface.

REFERENCES AND NOTES

1. Kobayashi, S.; Uyama, H.; Lee, S. W.; Matsumoto, Y. J Polym Sci Part A: Polym Chem 1993, 31, 3133–3139.
2. Uyama, H.; Honda, Y.; Kobayashi, S. J Polym Sci Part A: Polym Chem 1993, 31, 123–128.
3. Akashi, M.; Chao, D.; Yashima, E.; Miyauchi, N. J Appl Polym Sci 1990, 39, 2027–2030.
4. Brown, R.; Stützel, B.; Sauer, T. Macromol Chem Phys 1995, 196, 2047–2064.
5. Kawaguchi, S.; Winnik, M. A.; Ito, K. Macromolecules 1995, 28, 1159–1166.
6. Lacroix-Desmazes, P.; Guyot, A. Polym Bull 1996, 37, 183–189.
7. Furuhashi, H.; Kawaguchi, S.; Itsuno, S.; Ito, K. Colloid Polym Sci 1997, 275, 227–233.
8. Capek, I.; Riza, M.; Akashi, M. J Polym Sci Part A: Polym Chem 1997, 35, 3131–3139.
9. Liu, J.; Gan, L. M.; Chew, C. H.; Quek, C. H.; Gong, H.; Gan, L. H. J Polym Sci Part A: Polym Chem 1997, 35, 3575–3583.
10. Liu, J.; Chew, C. H.; Gan, L. M.; Teo, W. K.; Gan, L. H. Langmuir 1997, 13, 4988–4994.
11. Chen, M.-Q.; Serizawa, T.; Kishida, A.; Akashi, M. J Polym Sci Part A: Polym Chem 1999, 37, 2155–2166.
12. Chen, M.-Q.; Kishida, A.; Serizawa, T.; Akashi, M. J Polym Sci Part A: Polym Chem 2000, 38, 1811–1817.
13. Tuncel, A. Polymer 2000, 41, 1257–1267.
14. Kawaguchi, S.; Tano, K.; Maniruzzaman, M.; Ito, K. Macromol Symp 2000, 150, 101–108.
15. Chudej, J.; Guyot, A.; Capek, I. Macromol Symp 2002, 179, 241–256.
16. Shen, R.; Akiyama, C.; Senyo, T.; Ito, K. C R Chimie 2003, 6, 1329–1335.
17. Akashi, M.; Yanagi, T.; Yashima, E.; Miyauchi, N. J Polym Sci Part A: Polym Chem 1989, 27, 3521–3530.
18. Ito, K.; Sabao, K.; Kawaguchi, S. Macromol Symp 1995, 91, 65–72.
19. Ishizu, K.; Tahara, N. Polymer 1996, 37, 2853–2856.
20. Ishizu, K.; Yamashita, M.; Ichimura, A. Polymer 1997, 38, 5471–5474.
21. Riza, M.; Tokura, S.; Kishida, A.; Akashi, M. New Polym Mater 1994, 4, 189–198.
22. Amalvy, J. I.; Unali, G.-F.; Li, Y.; Granger-Bevan, S.; Armes, S. P. Langmuir 2004, 20, 4345–4354.
23. Neri, P.; Antoni, G.; Benvenuti, F.; Cocola, F.; Gazzei, G. J Med Chem 1973, 16, 893–897.
24. Nakato, T.; Tomida, M.; Suwa, M.; Morishima, Y.; Kusuno, A.; Kakuchi, T. Polym Bull 2000, 44, 385–391.
25. Suwa, M.; Hashidzume, A.; Morishima, Y.; Nakato, T.; Tomida, M. Macromolecules 2000, 33, 7884–7892.
26. Kang, H. S.; Yang, S. R.; Kim, J.-D.; Han, S.-H.; Chang, I.-S. Langmuir 2001, 17, 7501–7506.
27. Nakashima, T.; Yamada, Y.; Yoshizawa, H. Colloid Polym Sci 2007, 285, 1487–1493.

Colloid Polym Sci (2009) 287:525–532
DOI 10.1007/s00396-009-1998-z

ORIGINAL CONTRIBUTION

Design of polylactide-grafted copolymeric stabilizer for dispersion polymerization of D,L-lactide

Makoto Muranaka · Hidekazu Yoshizawa · Tsutomu Ono

Received: 27 October 2008 / Revised: 22 December 2008 / Accepted: 28 December 2008 / Published online: 22 January 2009

Abstract Poly(D,L-lactide) (PDLLA) microspheres with narrow diameter distribution were prepared by dispersion polymerization of D,L-lactide in xylene/heptane (1:2, *v/v*) using poly(dodecyl methacrylate)-*g*-poly(D,L-lactide) (PDMA-*g*-PDLLA) as a dispersion stabilizer. The particle diameters of PDLLA microspheres were controlled from 200 nm to 5 μm by altering the concentration and the graft chain number of PDMA-*g*-PDLLA. The effect of the copolymer composition on the particle diameter was investigated to clarify an important factor of the copolymer structure for the control of the particle diameter. As a result, it was necessary for anchor block in diblock copolymer as a dispersion stabilizer to have low solubility in the solution rather than the compatibility with particles. Moreover, we confirmed by dynamic light scattering measurement that PDMA-*g*-PDLLA formed micelles in the solution. In conclusion, it was clarified that PDLLA microspheres with a wide range of particle diameter were prepared due to the different kinetic stability of micelles.

Keywords Poly(D, L-lactide) · Microsphere · Dispersion polymerization · Graft copolymeric stabilizer · Copolymeric micelles

Introduction

Heterogeneous polymerization has been of increasing interest for the last three decades, due to the simple preparation of polymeric microspheres with narrow diameter distribution and a wide range of particle diameter [1]. This technique is classified into two methods. The first is emulsion polymerization, which is able to prepare the polymeric microspheres with submicrometer size using reaction medium not dissolving almost monomer. The polymerization takes place in the micelles composed of monomer and emulsifier. The second is dispersion polymerization, which is able to prepare the polymeric microspheres with micrometer size using reaction medium dissolving monomer but not dissolving polymer. The polymerization takes place in reaction medium until the polymer reaches critical molecular weight to precipitate, then the precipitated particles are stabilized by a dispersion stabilizer.

In dispersion polymerization, the dispersion stabilizer which affects the stability of the precipitated particles plays an important role for microsphere preparation. Many workers have prepared monodisperse polymeric microspheres using homopolymeric stabilizers such as poly(vinyl pyrrolidone) and hydroxypropyl cellulose [2–4]. They found that smaller microspheres were obtained at a higher dispersion stabilizer concentration and molecular weight. On the other hand, Dawkins and coworkers have made near-monodisperse polymeric microspheres using diblock copolymeric stabilizer such as poly(styrene-*b*-ethylene-*co*-propylene) and poly(styrene-*b*-dimethylsiloxane) [5–8]. They have investigated the effect of the molecular structure in diblock copolymer such as molecular weight and the alkyl group number of anchoring block on the resultant particle diameter. Winnik et al. confirmed the existence of regular micelles comprising several hundred diblock copolymers and micellar clusters corresponding to the aggregate of tens of micelles in aqueous solution by dynamic light scattering measurement [9–10]. They also

M. Muranaka · H. Yoshizawa · T. Ono (✉)
Department of Material and Energy Science,
Graduate School of Environmental Science, Okayama University,
3-1-1 Tsushima-Naka,
Okayama 700-8530, Japan
e-mail: tono@cc.okayama-u.ac.jp

described that block copolymer with low molecular weight should be used as a stabilizer for dispersion polymerization of styrene in methanol to prepare large and monodisperse microspheres [11].

On the other hand, there have been few papers describing the use of graft copolymer as a stabilizer in dispersion polymerization. Slomkowski et al. reported that Poly(D,L-lactide) (PDLLA) and poly(L,L-lactide) (PLLA) microspheres with narrow diameter distribution were prepared by dispersion polymerization of D,L-lactide and L,L-lactide using poly(dodecyl acrylate)-*g*-poly(ε-caprolactone) as a dispersion stabilizer, respectively [12–13]. They investigated the critical micelle concentration (cmc) of the dispersion stabilizer in 1,4-dioxane/heptane (1:4, *v/v*) as a reaction medium. The polymerization occurred at lower concentrations than its cmc, it was found that the particle diameter and the diameter distribution depend on the molecular structures of the dispersion stabilizer [14]. We have also reported that PDLLA microspheres with narrow diameter distribution were prepared by PLLA-grafted copolymer, poly(dodecyl methacrylate)-*g*-poly(L,L-lactide) (PDMA-*g*-PLLA), as a dispersion stabilizer [15]. In this work, we investigated the effect of the molecular structures in PDMA-*g*-PDLLA on the particle diameter of PDLLA microspheres prepared by dispersion polymerization of D,L-lactide in xylene/heptane (1:2, *v/v*) to clarify an important factor of molecular structures in the graft copolymeric stabilizer for the control of the particle diameter.

Experimental

Materials

D,L-lactide purchased from Purac Biochem BV (Gorinchem, The Netherlands) was purified by the recrystallization from toluene. 2-Hydroxyethyl methacrylate (HEMA) and dodecyl methacrylate (DMA) purchased from Wako Pure Chemical Industries was purified by the distillation under reduced pressure. Toluene, xylene, and heptane (dehydrated-grade) were purchased from Wako Pure Chemical Industries were treated with 4 Å molecular sieves to remove dissolved water. PME-4000, poly(ethylene glycol) macromonomer (MA-PEG), was kindly provided by NOF. FM-0721, polydimethylsiloxane macromonomer (MA-PDMS), was purchased from Chisso were used as received. Other reagents were purchased from Wako Pure Chemical Industries and used as received.

Measurements

Gel permeation chromatography (HLC 8120, Tosoh, GPC) was performed on the basis of the polystyrene standards with tetrahydrofuran as an eluent to determine the number-averaged molecular weight (*Mw*) and the polydispersity index (*Mw/Mn*) of synthesized polymer. ^{1}H NMR (AL300 SC-NMR, JEOL) measurement was conducted using $CDCl_3$ as a solvent and tetramethylsilane (TMS) (1%, *v/v*) as an internal standard to determine the molecular structure of synthesized polymer. Scanning electron microscopic observation (S-4700, Hitachi, SEM) was performed to determine the particle diameter (*dp*) and the diameter distribution (coefficient of variation, CV) of prepared PDLLA microspheres. Differential scanning calorimetric measurement (SSC5200H, Seiko Instruments, DSC) was conducted to determine the glass transition temperature (T_g) of PDMA-*g*-PDLLA and PDLLA microspheres. The heating rate was kept at 5 K/min, and the atmospheric temperature was scanned from 253 K to 373 K. Dynamic light scattering measurement (FPAR-1000, Otsuka Electronics, DLS) was carried out at 293 K to determine the hydrodynamic diameter (R_h) of micelles that consist of PDMA-*g*-PDLLA in xylene/heptane (1:2, *v/v*).

Synthesis

PDMA-g-PDLLA

The preparation of PDMA-*g*-PDLLA serves as a typical example for PDLLA-grafted copolymer. MA-PDLLA was synthesized by ring-opening polymerization of D,L-lactide using HEMA as an initiator in the presence of stannous 2-ethylhexanoate as a catalyst [16]. MA-PDLLA (*Mw*= 3,700, 0.42 mmol), DMA (9.65 mmol), and dehydrated toluene 18 ml as a solvent were placed into a round-bottom reactor. After nitrogen was admitted to remove oxygen, the reactor was immersed in an oil bath at 358 K. Dehydrated toluene dissolving benzoyl peroxide (BPO) (0.63 mmol) was added to initiate the polymerization. The polymerization was conducted for 3 h. After the polymerization, the reaction mixture was poured into excess methanol to remove DMA. The precipitate was recovered and added to 1,4-dioxane/heptane (1:4, *v/v*) to remove the remaining MA-PDLLA. After the purification, the polymer was dried under reduced pressure at 313 K.

The number of PDLLA chains in PDMA-*g*-PDLLA, *CN*, was calculated from the ^{1}H NMR spectrum using the integration ratio of DMA and PDLLA unit. It was defined by the following equation:

$$S_{\mathrm{MA-PDLLA}} = \frac{A_{\mathrm{MA-PDLLA}}}{\mathrm{PD}}$$

$$S_{DMA} = \frac{A_{DMA}}{2}$$

where $A_{\mathrm{MA\text{-}PDLLA}}$ and A_{DMA} denote the peak areas of CH for PDLLA unit of MA-PDLLA and $COOCH_2$ for DMA

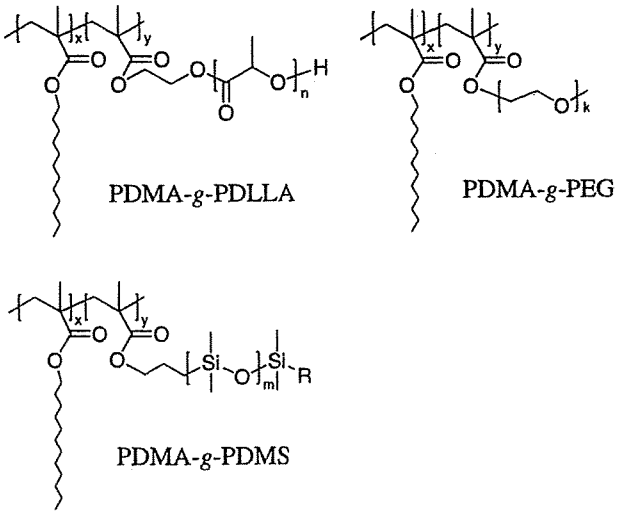

Fig. 1 Chemical structures of the graft copolymeric stabilizers

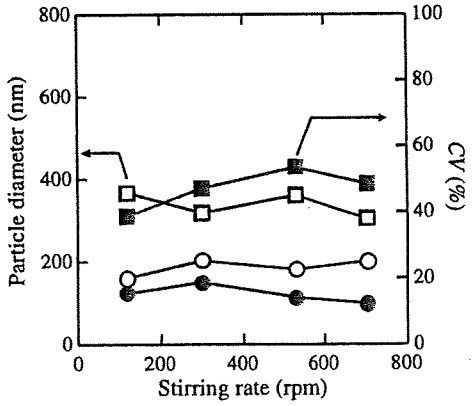

Fig. 2 Effect of stirring rate on the particle diameter and the diameter distribution of PDLLA microspheres prepared using (*open square*, *close square*) G_2 and (*open circle*, *close circle*) G_4 copolymers with different molecular structures; [PDMA-*g*-PDLLA]=10 g/l

unit in ^{1}H NMR spectrum of PDMA-*g*-PDLLA, respectively. And PD denotes the polymerization degree of MA-PDLLA. The number of DMA unit per MA-PDLLA unit, *N*, was defined by

$$N = \frac{S_{DMA}}{S_{MA-PDLLA}}$$

$$CN = \frac{Mw_{copolymer}}{(Mw_{DMA} \cdot N + Mw_{MA-PDLLA})}$$

where $Mw_{copolymer}$, Mw_{DMA}, and $Mw_{MA\text{-}PDLLA}$ denote the weight-averaged molecular weight of PDMA-*g*-PDLLA, DMA, and MA-PDLLA, respectively.

PDMA-g-PEG

MA-PEG (*Mw*=4,200, 0.55 mmol), DMA (14.49 mmol), and dehydrated toluene 18 ml as a solvent were placed into a round-bottom reactor. After nitrogen was admitted to remove oxygen, the reactor was immersed in an oil bath at 358 K. Dehydrated toluene dissolving BPO (0.47 mmol) was added to initiate the polymerization. The polymerization was conducted for 3 h. After the polymerization, the reaction mixture was poured into excess methanol to remove the remaining MA-PEG and DMA, and then the precipitate was recovered. After the purification, the polymer was dried under reduced pressure at 313 K.

PDMA-g-PDMS

MA-PDMS (*Mw*=8,400, 7.96 mmol), DMA (7.96 mmol), and dehydrated toluene 18 ml as a solvent were placed into a round-bottom reactor. After nitrogen was admitted to remove oxygen, the reactor was immersed in an oil bath at 358 K. Dehydrated toluene dissolving BPO (0.94 mmol) was added to initiate the polymerization. The polymerization was conducted for 3 h. After the polymerization, the reaction mixture was poured into excess methanol. The precipitate was recovered and added to methanol/2-propanol (1:2, *v/v*) to remove the remaining MA-PDMS. After the purification, the polymer was dried under reduced pressure at 313 K.

Table 1 Molecular structures of PDMA-*g*-PDLLA

Code	Graft copolymer	Mw^a	Mw/Mn^b	Macromonomer		N^e	CN^f (PDLLA)
				Mw^c	Mw/Mn^d		
G_1	PDMA-*g*-PDLLA	41,300	2.31	3,700	1.30	116	1.3
G_2	PDMA-*g*-PDLLA	34,500	2.23	3,700	1.30	54	2.0
G_3	PDMA-*g*-PDLLA	36,500	2.04	3,700	1.30	27	3.4
G_4	PDMA-*g*-PDLLA	30,700	2.53	6,600	1.40	24	2.4

[a,b,c,d] Determined by GPC
[e] Number of DMA units per MA-PDLLA unit
[f] A grafted PDLLA chain number in a copolymer

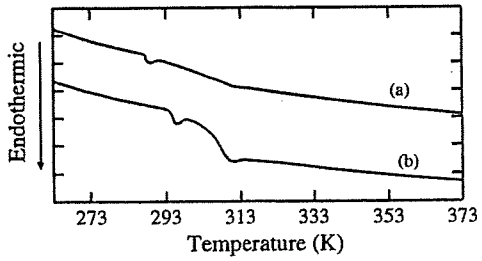

Fig. 3 DSC curves for (*a*) G_4 copolymer and (*b*) PDLLA microspheres prepared with G_4 copolymer; [PDMA-*g*-PDLLA]=10 g/l

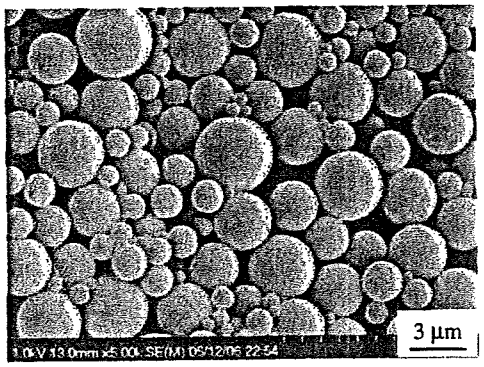

Fig. 4 SEM image of PDLLA microspheres prepared with PDMA-*g*-PEG as a dispersion stabilizer; (*dp*=1,420 nm, CV=48.2%), [PDMA-*g*-PEG]=10 g/l

Preparation of PLA microspheres

The preparation of PDLLA microspheres is shown as a typical example. D,L-lactide (0.5 g, 3.47 mmol) was added into 17 ml of dehydrated xylene/heptane (1:2, *v/v*) dissolved PDMA-*g*-PDLLA. In this study, the concentration of dispersion stabilizer ranged from 0.01 to 0.2 g. The solution was stirred at 120 rpm with a magnetic stirrer. Three milliliters of dehydrated xylene/heptane (1:2, *v/v*) dissolving stannous 2-ethylhexanoate (0.0475 g, 0.12 mmol) as a catalyst and lauryl alcohol (0.011 g, 0.06 mmol) as an initiator was prepared. The solution was added with a syringe and the polymerization was conducted at 368 K for 9 h. After the polymerization, the reaction solution was poured into excess cold heptane. The solution was centrifuged for 5 min at 9,000 rpm and the microspheres were redispersed into excess heptane. The solution was filtered to obtain the prepared microspheres.

Results and discussion

Synthesis of PDMA-*g*-PDLLA

Figure 1 shows the chemical structures of synthesized graft copolymers with different grafted polymer chains. MA-PDLLA was synthesized by ring-opening polymerization of D,L-lactide using HEMA as an initiator. Subsequently, MA-PDLLA was copolymerized with DMA by free radical polymerization using BPO as an initiator to obtain PDMA-*g*-PDLLA. The ^{1}H NMR spectrum of PDMA-*g*-PDLLA had peaks in the range of 1.5–1.7 ppm (CH_3 for PDLLA unit), 5.1–5.3 ppm (CH for PDLLA unit) and around 3.9 ppm ($COOCH_2$ for DMA unit). Furthermore, peaks at 5.6 and 6.2 ppm (CH_2=CH for MA-PDLLA) were not detected in the spectrum. Therefore, PDMA-*g*-PDLLA was finally identified. The molecular structures of synthesized PDMA-*g*-PDLLA were summarized in Table 1.

Synthesis of PDMA-*g*-PEG

PDMA-*g*-PEG was synthesized by free radical polymerization of DMA and MA-PEG as a macromonomer using BPO as an initiator. The ^{1}H NMR spectrum of PDMA-*g*-PEG had peaks in the range of 3.6 ppm ($COOCH_2CH_2$ for PEG unit) and around 3.9 ppm ($COOCH_2$ for DMA unit). Furthermore, peaks at 5.5 and 6.1 ppm (CH_2=CH for MA-PEG) were not detected in the spectrum. Therefore, PDMA-*g*-PEG was finally identified. The MA-PEG number in PDMA-*g*-PEG, *CN*, was calculated by the similar method to PDMA-*g*-PDLLA.

Synthesis of PDMA-*g*-PDMS

PDMA-*g*-PDMS was synthesized likewise using MA-PDMS. The ^{1}H NMR spectrum of PDMA-*g*-PDMS had

Table 2 Molecular structures of graft copolymeric stabilizers

Graft copolymer	*Mw*[a]	*Mw/Mn*[b]	Macromonomer		*N*[c]	*CN*[f] (Macromonomer)
			Mw[c]	*Mw/Mn*[d]		
PDMA-*g*-PEG	27,500	2.38	4,200	1.09	22	2.8
PDMA-*g*-PDMS	39,000	2.05	8,400	1.11	23	2.8

PEG poly(ethylene glycol), *PDMS* poly(dimethyl siloxane)
[a,b,c,d] Determined by GPC
[e] Number of DMA units per macromonomer unit
[f] A grafted macromonomer chain number in a copolymer

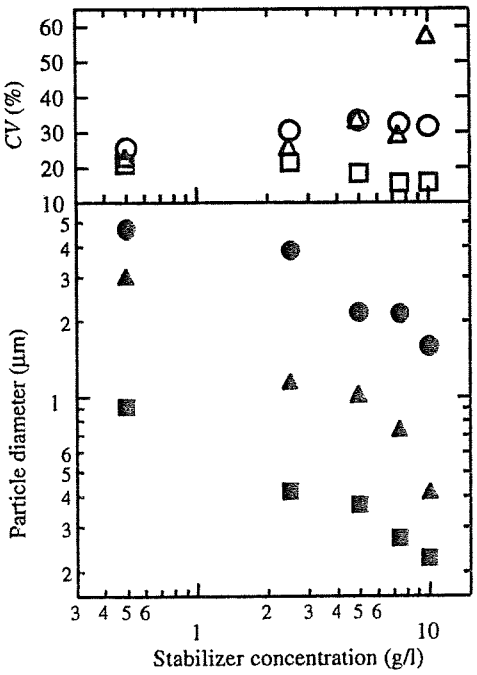

Fig. 5 Effect of concentration of (*open circle, close circle*) G_1, (*open triangle, close triangle*) G_2, and (*open square, close square*) G_3 copolymers with different number of graft chains on the particle diameter and the diameter distribution of PDLLA microspheres

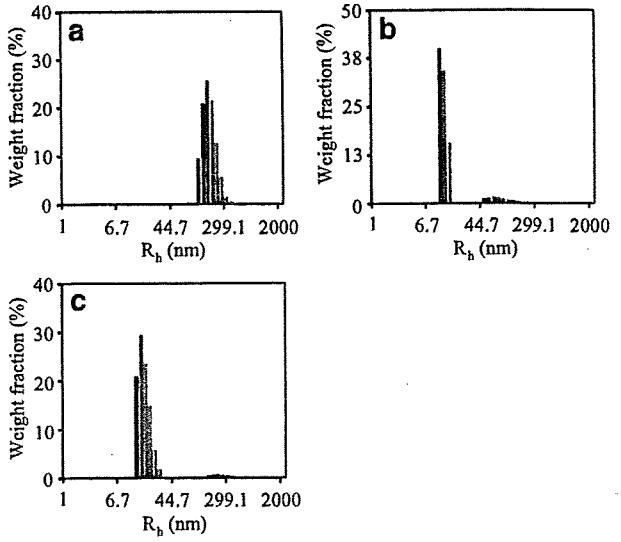

Fig. 7 Size distributions for micellar aggregates of a G_1 (R_h=194 nm), b G_2 (R_h=13 nm, 93 nm) and c G_3 (R_h=18 nm, 276 nm) copolymers in xylene/heptane (1:2, *v/v*) at 293 K; [PDMA-*g*-PDLLA]=10 g/l

peaks in the range of 0.0 ppm ($Si(CH_3)_2$ for PDMS unit) and around 3.9 ppm (OCH_2 for DMA unit). Furthermore, peaks at 5.4 and 6.0 ppm (CH_2=CH for MA-PDMS) were not detected in the spectrum. Therefore, PDMA-*g*-PDMS was also finally identified. The MA-PDMS number in PDMA-*g*-PDMS, *CN*, was calculated likewise.

Fig. 6 SEM images of PDLLA microspheres using a G_1 (*dp*= 1,600 nm, CV=31.6%), b G_2 (*dp*=414 nm, CV=57.2%), and c G_3 (*dp*=225 nm, CV=15.8%) copolymers. They have different number of graft chains; [PDMA-*g*-PDLLA]=10 g/l

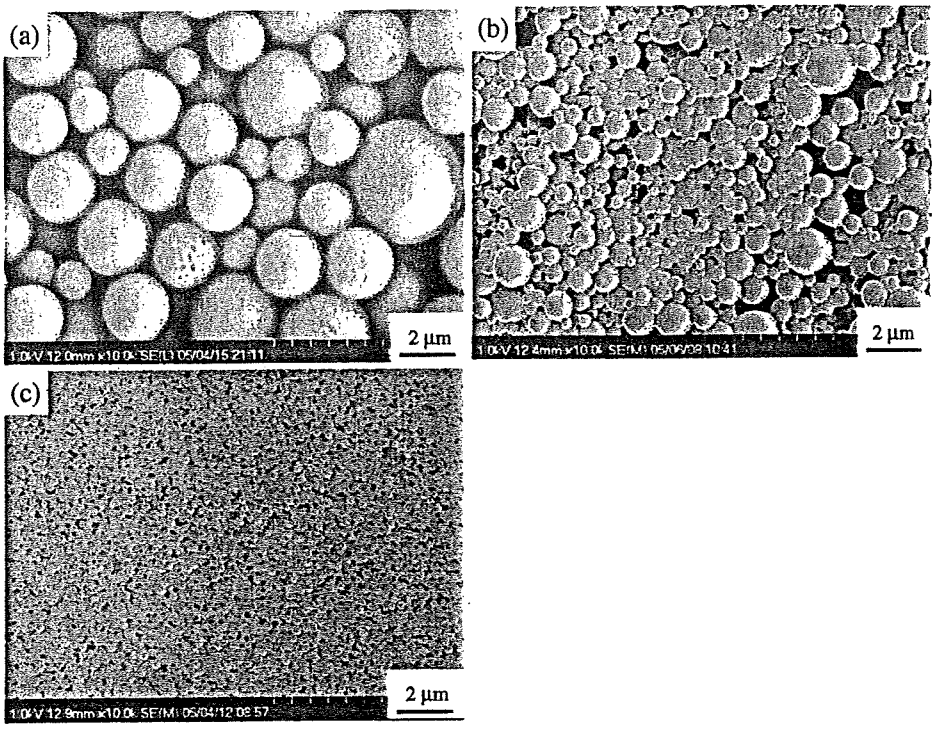

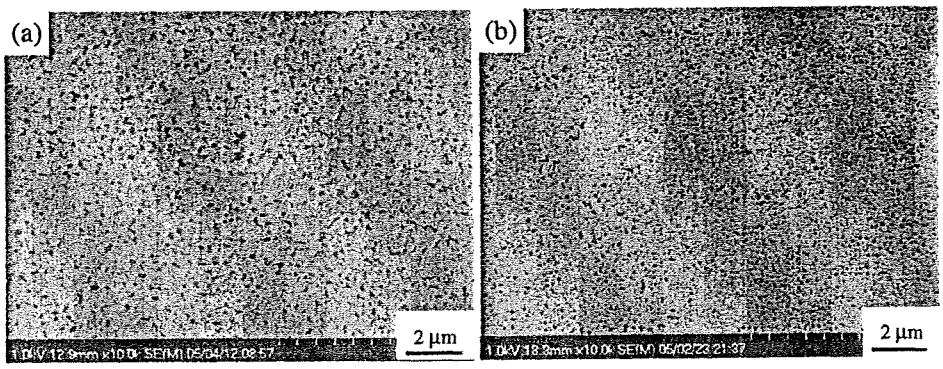

Fig. 8 SEM images of PDLLA microspheres using **a** G_3 (dp=225 nm, CV=15.8%) and **b** G_4 (dp=160 nm, CV=15.4%) copolymers. They have different graft chain length; [PDMA-*g*-PDLLA]=10 g/l

Effect of stirring rate

Figure 2 shows the effect of the stirring rate in the solution on the particle diameter of PDLLA microspheres prepared using G_2 and G_4 copolymers with different molecular structures. As shown in this figure, the stirring rate did not affect the particle diameter.

In addition, in the case with G_2 copolymer, the particle diameter exhibited larger than that in the case with G_4 copolymer. This result implied that the adsorption rate of G_4 copolymer was larger than that of G_2 copolymer because G_4 copolymer shows lower solubility in the solution than G_2 copolymer. As a result, G_4 copolymer prevented primary particles from further aggregation, leading to the formation of small particles with narrow diameter distribution. Thus, it was suggested that the particle diameter depended on the adsorption rate of PDMA-*g*-PDLLA on the surface of primary particles. Namely, it was expected that the particle diameter of PDLLA microspheres was controlled by the molecular structures in PDMA-*g*-PDLLA.

The surface characterization of polymeric microspheres prepared by dispersion polymerization using a dispersion stabilizer with nitrogen element has been performed with X-ray photoelectron spectroscopy (XPS) and Fourier transform infrared spectroscopy (FT-IR) [17–18]. They exhibited the existence of diblock copolymeric stabilizer immobilized on the surface of the polymeric microspheres. For PDMA-*g*-PDLLA, however, XPS and FT-IR are not available. Therefore, we confirmed the existence of PDMA-*g*-PDLLA with ^{1}H NMR. Moreover, we also confirmed the T_g based on PDMA-*g*-PDLLA with DSC. Figure 3 shows the DSC curves of G_4 copolymer and PDLLA microspheres prepared by dispersion polymerization with G_4 copolymer. From this figure, T_g based on PDMA in G_4 copolymer was 287 K. In addition, T_g of G_4 copolymer was confirmed from the DSC curve of the resultant PDLLA microspheres and the T_g shifted higher to 294 K. Therefore, it was suggested that PDLLA anchor blocks in G_4 copolymer were strongly adsorbed on surface of the primary particles.

Effect of graft chain structure

We investigated the effect of the molecular structures in PDMA-*g*-PDLLA on the particle diameter to clarify an important factor of the molecular structure for the adsorption on the surface of primary particles. As the first point, Ober et al. reported that the anchor block in copolymeric stabilizer should be compatible with the particles [19]. In contrast, Baines et al. suggested that the compatibility was not an essential requirement [20]. We synthesized copolymers with different grafted polymer chains to experimentally prove the point mentioned above. PDLLA and PDMS bring hydrophobicity to the copolymer but PEG brings hydrophilicity. In addition, PDLLA and PEG show low solubility in xylene/heptane (1:2, *v/v*) during dispersion polymerization. In contrast, PDMS shows high solubility in the solution. The characteristics of the synthesized graft copolymers were summarized in Table 2. Figure 4 shows the SEM image of PDLLA microspheres prepared by dispersion polymerization with PDMA-*g*-PEG as a stabilizer. As a result, in cases with PDMA-*g*-PDLLA and PDMA-*g*-PEG, PDLLA microspheres were prepared. Thus, PDMA-*g*-PEG played a role of a dispersion stabilizer even PEG chain brought no good compatibility with PDLLA particles. In contrast, PDMA-*g*-PDMS gave rise to an undefined-shaped product in the solution even PDMS chain had better compatibility with PDLLA particles than PEG chain. In conclusion, it is necessary for an anchor block in diblock copolymer as a dispersion stabilizer to have low solubility in the solution rather than the compatibility with particles.

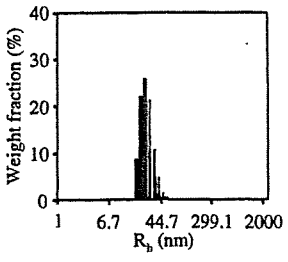

Fig. 9 Size distribution for micellar aggregates of G_4 copolymer in xylene/heptane (1:2, *v/v*) at 293 K; R_h=24 nm, [PDMA-*g*-PDLLA]=10 g/l